Hindawi
International Transactions on Electrical Energy Systems
Volume 2023, Article ID 4690844, 23 pages
https://doi.org/10.1155/2023/4690844

Research Article

Investigation on Energy Flow Performance of a Photovoltaic/Battery-Based Isolated Charging Station for Battery-Powered Electric Vehicles

Abdelsalam A. Ahmed,[1] Mohamed G. Hussien ,[1,2] and Yasmine Marzouk Abo-Elyzeed[3]

[1]*Electrical Power and Machines Engineering Department, Faculty of Engineering, Tanta University, Tanta, Egypt*
[2]*School of Mechanical Engineering and Automation, Harbin Institute of Technology (Shenzhen), Shenzhen, China*
[3]*Electrical Power and Machines Engineering Department, Higher Institute of Engineering, El-Shorouk Academy, Cairo, Egypt*

Correspondence should be addressed to Mohamed G. Hussien; mohamed.hussien3@f-eng.tanta.edu.eg

Received 4 March 2023; Revised 4 June 2023; Accepted 21 September 2023; Published 10 October 2023

Academic Editor: Salvatore Favuzza

Researchers are paying attention to the current trend of electric vehicles (EVs), but there are not many places to charge them and serve as electric vehicle charging stations (EVCSs). In order to prevent the lack of EVCS for battery EVs (BEVs) on any road with all modes of operation, this paper proposed the design of a novel configuration and control structures for the isolated charging station (ICS) based on the solar PV system for efficient energy utilization to charge battery EVs (BEVs) with flexible double function cascaded converter (MPPT and DC-link voltage regulation). This was done with the aid of a battery energy storage system (BESS) as a backup/auxiliary source. The PV system is reliant on solar radiation and the daily load profile. Therefore, the BESS is employed to provide continuous power to BEVs and overcome PV's intermittent nature. The cascaded converter is used to achieve the MPP and to regulate the DC-link voltage to its reference value (100 V), while the buck-boost matching bidirectional DC-DC voltage converters (MBDVCs) are used for charging and discharging mode/buck and boost mode, respectively, of BEVs and BESSs. Additionally, the MBDVCs are used as an interface between the ICS sources with the load through the developed control systems. The outcomes of various operating modes show that the system functions effectively. To verify the system performance, the MATLAB/Simulink application builds the system setup.

1. Introduction

In numerous industrial applications, hybrid PV modules and battery storage packs have been incorporated. This system is applied to electric vehicles (EVs), the grid, and standalone applications. Initially, the applications of this system are examined yearly to ascertain and close the gap in this paper.

Maintaining the common DC bus voltage within a reasonable range is essential for a charging microgrid to function. The plug-in EVs (PEVs) are regarded as a power terminal of the system since they are a variable DC load and photovoltaic-based production is a no dispatchable (variable) generation. As a slack terminal, the electric station unit (ESU) (station battery) is in charge of balancing the power surplus/deficit brought on by power terminals and ensuring stable system functioning [1]. When connected to a DC bus system, many elements (loads, energy storage devices, and renewable resources) work as intended, although there are challenges with maintaining consistent operation with renewable sources [2]. As a result, appropriate controllers must be developed to achieve the best performance from solar arrays, energy storage systems, electric vehicles (EVs), and loads that are connected to DC buses.

The energy management system (EMS) of an electric vehicle is activated immediately using a hybrid PV/battery multisource power supply [3]. PV serves as the major power source and battery serves as the secondary energy storage device in [4]. By taking into account PV as a power source, lead acid battery as a storage device, and DC load, the

charging process of PEVs is investigated for a DC microgrid using I-V and average SMC techniques. For the purpose of delivering continuous charging and uninterruptible supply to the household loads, reference [5] covers the multimode operation of a photovoltaic (PV) array, a battery, the grid, and the diesel generator (DG) set-based charging station (CS). According to proven experimental data, the authors of [6] proposed EVCS for charging Carryall 6 EVs. Additionally, the EVCS or charger is installed to charge the majority of necessary hardware for the E-Scooter [7].

The planning methodology for EVCS with better station location is included in the publication [8]. A review of the location of EVCS and its impact on the network of distribution stations is provided in [9]. A thorough analysis of EVCS, including the best sites, methods for sizing them, modelling, charging methodologies, transport networks, modes of transportation, data processing, sources of the various data types, and stakeholders, is given in [10]. In [11], the authors present a grid-connected CS without any renewable source; only grid is used to supply energy to EVs without including V2G like our work. However, OGCS's control cannot maintain constant DC-link voltage without reactive power compensation. The authors introduced FCEV dynamically which consists of HPS (fuel cell and ultracapacitor) to investigate the DC-link voltage [12]. As conclusion, the results reflect the correctness of proposed control system. This research [13] proposed multiobjective two-stage optimization for grid-connected EVCS which included the three main aspects, that is, economic, energy, and environmental. The results show how the proposed method reduces the emission to 32%, and operation cost is reduced by 30%, and total energy consumption is reduced by 15%.

In [14], a comparison between conventional fuel vehicle and EV is presented including comparative items of energy consumption and CO_2 emission. Finally, the results show that the energy consumption of EV is less than conventional vehicle by 8 times and the CO_2 emissions from EVs are, at least, 10 times lower over a period of 15 years. In [15], a grid-connected electric vehicle charging station assisted by photovoltaic with battery pack is presented to manage all power sources of station for achieving the correct charging system under different irradiance conditions. Also, the authors considered the energy transmission cost and state of charge (SOC). In [16], the authors proposed a design model of grid-connected electric vehicle charging stations based on renewable energy sources (PV) to provide continuous charging for electric vehicles. The research in [17] provided EMS for grid-connected electric vehicles in commercial area to manage the power among all station sources (PV, battery pack, and grid) for achieving maximum efficiency and reducing operational cost. In [18], the authors proposed a novel configuration of off-grid fast EV charging station based on PV array of two design reflectors to make the system more efficient. The research in [19] presented all possible modes of operation of grid-connected EV charging station under current control bidirectional converters with vector control. In [20], the authors provided an optimized PV system for charging EVs in University of Technology Malaysia (UTM).

The research in [21] introduced a grid-connected ultra-fast EV charging high gain step-up SEPIC converter with three power switches and only two duty ratios. Also, it proposed the HSFNA-based MPPT tracker which provides fast convergence, accurate response, and minor complication. The simulated and experimental results prove the correctness of the proposed ultra-fast charging system for EVs. Also, reference [22] presented a grid-connected PV system with new MPPT method (an adaptive TS-fuzzy-based RBF neural network) for maximizing energy utilization with improved performance as compared to the conventional MPPT methods. The authors in [23] proposed an inverter control strategy for single-stage grid-connected PV system (online CMPN-based AAFLC method) under varying operating conditions with rapid convergence velocity. The real implementation of the proposed system is done using dSPACE real time platform, and the results show how the system performs effectively. The work presented in [24] demonstrated the grid-tied PV system through the intelligent FPSO method for obtaining the maximum power from PV with experimental implementation using the interfaced dSPACE DS1104 with MATLAB/Simulink under variant ambient conditions. In addition to the modified SVPWM-based ripple, the compensator generates the required gating signals to control the inverter with analysis only. Reference [25] provided ANFIS-PSO for rapid, maximum power, and zero oscillation tracking for MPP of grid-connected PV system. The results show the effectiveness of the proposed method as compared to other methods. In [26], a grid tide of single stage of hybrid sources (PV and full cell) is presented based on Lyapunov function-based controller design to extract maximum power from hybrid renewable sources. The results highlight the correctness of the presented method during the steady state and dynamic state compared to the conventional method.

For rapid charging EV/PHEV converters, the research in [27] reviewed bidirectional converters and provided comparisons between three comparable converters for this purpose. Finally, the authors claimed that high battery side voltage results in high converter efficiency. Due to limitations, reference [28] selected low voltage battery packs for maintenance and safety reasons, compared three battery pack voltages (24 V, 48 V, and 300 V), and found that 48–60 V was the most promising option. The research in [29] proposed semi-bridgeless AC-DC converters in the front end to accelerate charging with 400 V DC voltage in order to circumvent the limiting low power for residential use (level 1 and level 2) in North America. The authors of [30] presented a grid-assisted PHEV/EV-based charging system (bidirectional converter). There are various charger kinds, and in this study [31], the authors provided an in-depth analysis of wireless EV charging systems and the various power electronics (PEs) designs. In [32], a grid-connected charging approach for EVs called the constant current constant voltage (CCCV) system is suggested with voltage-oriented regulation. With a CCCV profile, a novel resonant converter topology is proposed for charging EVs, and experimental findings are also provided [33]. The study in [34] presents an

overview of battery charger basics, pulse charging, and CCCV for Li-ion batteries with realization of linear and switching circuits. Reference [35] focused on the creation of a charging system for electric vehicles (EVs), which supplies power to the battery of the EV under various charging situations using distributed energy resources (DERs), such as a PV array and a battery storage system.

Although the BESS partially eliminates reliance on the grid, the authors in [36] offered a design of the PV system for charging EVs with BESS and their converters in the Netherlands. Therefore, this study fills this gap, eliminating grid dependency, but in different places where peak sun hours (PSHs) (as in Egypt) are 10 hours year-round, a backup source is available on its own in case of unforeseen circumstances. The EVCS of PV-powered-EVs is described in [37] to improve the advantages of employing renewable energy sources and decrease charging costs while lowering reliance on the grid. The ICS to charge EVs using a different charging profile (CC charging profile), but small-scale power system for one EV, was also presented in the study presented in [38]. However, using a large-scale power infrastructure, this work created an effective and secure CCCV charging profile.

The power flow to the EVs under the five operational modes is covered in this paper. These three power plants (the PV array, the EV's battery, and the station's battery) can interchange energy in all feasible ways. To handle the energy for that purpose, DC-DC converters are built and programmed. To utilize the sources for charging the vehicles with the greatest efficiency and in the shortest amount of time, both voltage control mode and current control mode are used. The suggested charging mechanism is validated through simulation in various operating scenarios. In Table 1, a comparison with similar studies is also noted.

This paper is organized as follows. The power plants for the planned PV-battery-based charging station are described and modelled in Section 2. The energy ratings of the PV and SS systems as well as the capacity of BEVs are used to determine the parameters of the buck-boost converter of PV, BEES, and PEVs in Section 3. In Section 4, each converter's control system, circumstances, and modes of operation are presented together with the power flow. The simulation's performance evaluation and findings are presented in Section 5. Section 6 introduces the paper's conclusion.

2. Description of Charging Station

2.1. System Configuration with EV Connected to DC Bus. As shown in Figure 1, the suggested system uses a battery as a secondary storage unit and PV as the primary power source. Another energy source is needed to make up for the photovoltaic source's infrequently available power output. A battery bank with sufficient power capacity is placed to give the system a constant power source in order to meet the fluctuating DC load needs. When the PV source produces more energy than it can store in the battery, the battery bank fills the gap. Likewise, when the PV source is unable to produce the necessary quantity of energy, the battery bank does so.

When the battery station is empty, the DC-link voltage is controlled by a cascaded buck DC converter in order to maximize the PV power. According to the described control system, a power buck-boost DC converter is used to charge and discharge the battery storage unit. Ten charging sockets, points, or outlets on the load side are intended to use buck-boost DC converters to charge EVs at various voltage levels. Electric vehicle batteries are often multiples of 72 V and 48 V. To prevent interruptions in the BESS's operation, two switches are utilized, as shown in Figure 2. One is directly linked to the DC link when the BESS is in the charging mode, and the other is connected to the middle of a cascaded buck converter when it is in the discharging mode.

2.2. Modelling of PV Array. PV models are needed for design and simulation purposes. A particularly precise mathematical model [39] that is ideal for circuit modelling is the one depicted in Figure 3(a). Equations can be used to represent the PV mathematical model as indicated by the relations below.

$$\begin{aligned} I_{\mathrm{pv}} &= I_{\mathrm{ph}} - I_D - I_{\mathrm{SH}}, \\ V_{\mathrm{pv}} &= V_d - R_s I_{\mathrm{pv}}, \\ I_{\mathrm{Ph}} - I_D - \frac{V_{\mathrm{pv}} + R_s I_{\mathrm{pv}}}{R_{\mathrm{sh}}} - I_{pv} &= 0, \\ I_D &= I_0\left(e^{V_{\mathrm{pv}}/V_T} - 1\right), \\ I_{Ph} &= \left[I_{sc} + K_i(\mathrm{T} - 298)\right]\frac{G}{1000}, \end{aligned} \tag{1}$$

where $K_i = 0.0017\ A/C$ is the cell's short circuit current temperature coefficient, I_{sc} is short circuit current of cell (A), and G is the solar radiation (W/m). The impact of temperature variation and wind speed is neglected.

2.3. Modelling of Battery. Lumped-parameter models are welcomed for the study of EV system integration, control, optimization, and the connectivity of EVs to off-grid charging stations. The battery terminal and general properties and dynamics, such as voltage, current, temperature, and SOC, are of more interest in those investigations than the specific electrochemical processes taking place inside the battery. In this work, the equivalent circuit model of the battery is used. As can be seen in Figure 3(b), the used battery's comprehensive electrical equivalent circuit model, the open circuit voltage (V_{oc}) is a function of SOC. Equations can be used to represent the mathematical model of a lithium-ion battery as shown by the relations below.

(i) Calculation of voltage drops:

Table 1: Comparison with related work.

Comparative items	Reference [2]	Reference [37]	Reference [38]	Proposed work
Design for charging EVs	Studied (rare details for 3 EVs)	Studied (rare details for 5 EVs)	Studied (few details for 1 EV)	Studied (all details for 10 EVs at the same time and 30 EVs/day)
System configuration	Grid connection	Grid connection	Standalone	Standalone
System efficiency	Not considered	Not calculated	Not calculated	Calculated
Charging profile	CCM and CVM (the best)	CC (the worst)	Stepped-CC (improved)	CCCV (the best)
Charging speed	Fast (≈2 hr)	Moderate (≈4–6 hr)	Not mentioned	Moderate (5 hr)
DC voltage regulation	Good	Not mentioned	Worst	Excellent
#Modes	Three modes	Unspecified	Three modes	Five modes

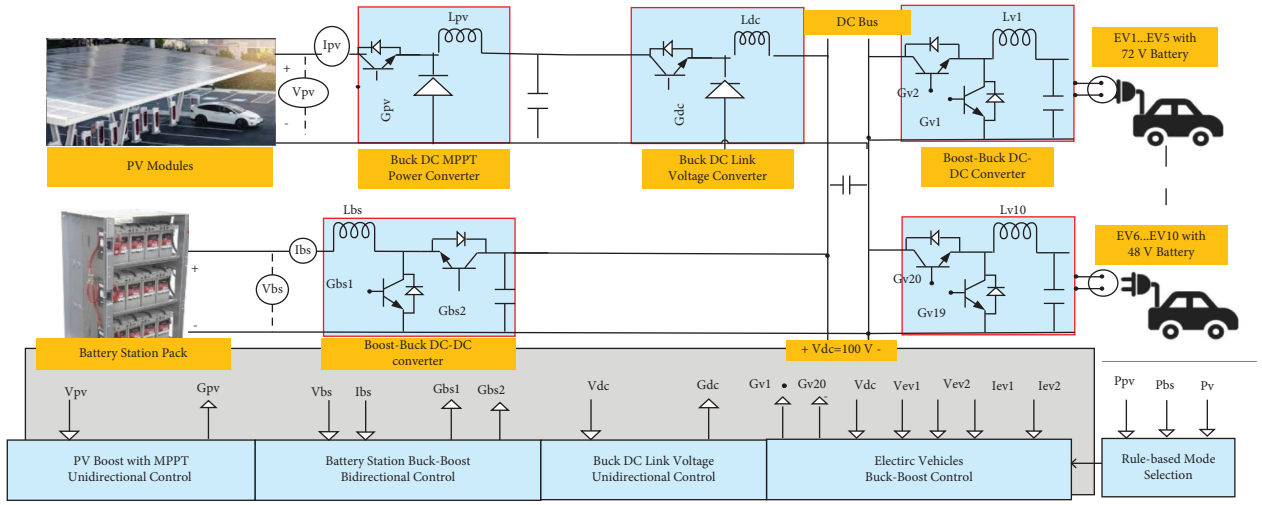

Figure 1: Schematic architecture for EV charging station: PV modules, standby energy storage battery, DC-DC converters, and batteries of EVs.

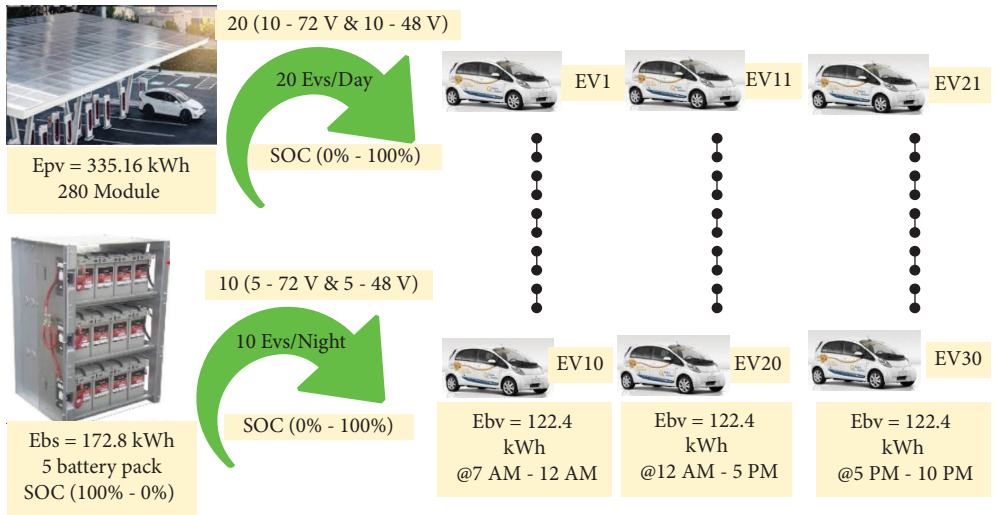

Figure 2: ICS ratings.

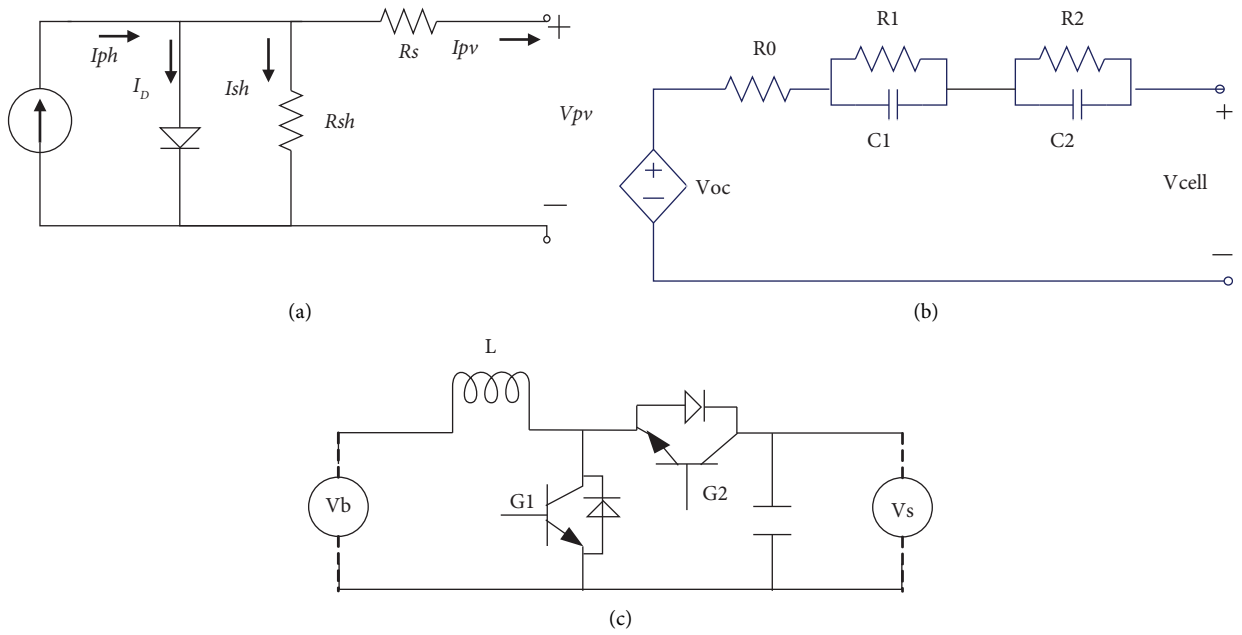

FIGURE 3: The equivalent circuits of the charging station are as follows: (a) PV modelling circuit, (b) battery equivalent circuit, and (c) buck-boost converter.

$$
\begin{aligned}
V0 &= i\mathrm{b} * R0,\\
V1 &= \int_0^t \left(\frac{\mathbf{ib}}{\mathbf{C1}}\right) - \left(\frac{\mathbf{V1}}{\mathbf{R1} * \mathbf{C1}}\right) \mathrm{d}t,\\
V2 &= \int_0^t \left(\frac{\mathbf{ib}}{\mathbf{C2}}\right) - \left(\frac{\mathbf{V2}}{\mathbf{R2} * \mathbf{C2}}\right) \mathrm{d}t,\\
V\mathrm{cell} &= Voc - V0 - V1 - V2,\\
Vb &= ns * V\mathrm{cell},\\
ib &= \frac{Ib}{np}.
\end{aligned}
\tag{2}
$$

In this model, no cooling system is considered (only natural air).

$$
T = \int_0^t \frac{ib(\mathrm{voc} - v\mathrm{cell}) - hA(T - \mathrm{Ten}) - bA\left(T^4 - \mathrm{Ten}^4\right)}{m * c} \mathrm{d}t,
\tag{3}
$$

where $V0$: voltage across internal resistance, $V1$: voltage across $R1$ $C1$, $V2$: voltage across $R2$ $C2$, Vcell: cell voltage, Vb: battery voltage, ib: battery current, ns: series cells, np: parallel cells, $m = 39g$ (cell mass), $c = 1\,w/g.k$ assumed for Li-ion cells in the range 0.9 to 1.02 cell capacity, $h = 4\,w/k.m^2$ assumed for free convection heat transfer, $A = 9.391 * 10^{-3}\,m^2$ (total surface area of the cell), and $b = 5.67 * 10^{-8}$ (Stefan–Boltzmann constant).

(ii) State of charge calculation:

The state of charge (SOC) is calculated as function of temperature and charging current as shown below:

$$
\begin{aligned}
\mathrm{soc} &= \mathrm{soc0} * e^{-5.738\,(1/T - 209.9 - 1/\mathrm{Tref} - 209.9)}\\
&\quad - \frac{1}{3600 * 1.1} * \int_{t1}^{t2} \mathrm{ib}\,\mathrm{d}t,
\end{aligned}
\tag{4}
$$

where SOC: current state of charge, SOC0: initial SOC, T: cell temperature, T_{ref}: reference temperature, i_b: battery cell current, and t: time.

2.4. Modelling of Buck-Boost DC-DC Converter. Figure 3(c) depicts the buck-boost converter modelling circuit, with the inductor side representing the battery side and the other side representing the DC-link side. DC-DC converters for PV work in bucking mode, whereas those for BESS work in boosting mode during discharging and bucking mode during charging. The latter mode is solely used for BEVs; V2G is not considered. In the parametric design stage for buck-boost converters, the input voltage range ($V_{\mathrm{in-min}}$ and $V_{\mathrm{in-max}}$), nominal output voltage (V_{out}), and maximum output current are required to compute the power stage.

3. Ratings and Parametric Design of Power Source, Energy Storage Units, and Converters

3.1. Load Estimation. For a given five-battery pack of each BEV ($72V - 240Ah$) in parallel with another five-battery pack of each BEV ($48V - 150Ah$), the total energy capacity of load is calculated as follows:

$$E_{\text{tot}} = (5 * 72 * 240) + (5 * 48 * 150) = 122.4\,kWh. \quad (5)$$

The mathematical equation of capacity of 72 V and 48 V is shown in equation (6) for compact design with two outlets/charging points.

$$E_{2\text{ev}} = (72 * 240) + (48 * 150) = 24.48\,kWh. \quad (6)$$

3.2. Component Sizing of PV System. The total number of PV modules is intended to simultaneously charge 10 EVs. Additionally, the PV modules are built to recharge the station's battery on days without moving vehicles or when there is a small load. The EVs are designed to charge for 5 hours from 0% to 100% SOC as the worst-case scenario, taking the average PSH in Egypt into account, to reduce the amount of space needed for PV. If the controlled charging time is decreased to a low value, the number of PV modules increases, and as a result, more space is needed for installation. We can decrease the charging time for fast charging if the grid side with PV is considered. The power capacity of the PV module P_{pv} for the two battery-powered vehicles is calculated using a derating factor of 90% and a converter's efficiency of 90% as shown in the following equation:

$$P_{\text{pv}} = \frac{E_{2\text{ev}}}{T_{\text{ch}} * \eta_{\text{pv}} * \eta_{\text{dc}} * \eta_{\text{BB}}} = \frac{24.48}{5 * 0.9^3} = 6.716\,kW, \quad (7)$$

where T_{ch} is the proposed charging time, η_{pv} is the PV converter efficiency, η_{dc} is the DC converter efficiency, and η_{BB} is the buck-boost converter efficiency. For rating of the PV module of 120 W, the number of the PV modules (N_{pv}) for the two battery vehicles is calculated as follows:

$$N_{\text{pv}} = \frac{P_{\text{pv}}}{P_{\text{pvm}}} = \frac{6.716}{0.12} = 55.967\ \text{Modules}. \quad (8)$$

So, there are 56 PV modules connected in parallel at rated voltage of 126 V and rated current of 0.95 A for the two BVs. The total number of the PV modules for the CS (N_{pv}_tot) is calculated as follows:

$$N_{\text{pv-tot}} = 56 * 5 = 280\ \text{Modules}. \quad (9)$$

3.3. Component Sizing of Battery Station. The station battery pack capacity E_{bs} of each $(72V - 480Ah) = 34.56$KWh is used as auxiliary/backup source with PV to charge BEVs. Note that all batteries are lithium-ion type. Each capacity of the two BEVs for the station *Ebs* and number of it could be calculated as follows:

$$E_{\text{bs}} = \frac{E_{2\text{ev}}}{\eta_{\text{pv}} * \eta_{\text{dc}} * \eta_{\text{BB}}} = \frac{24.48}{0.9^3} = 33.58\,\text{kWh}, \quad (10)$$

$$N_{\text{bs}} = \frac{E_{\text{bs}}}{E_{1\text{bs}}} = \frac{33.58}{34.56} = 0.972 \approx 1, \quad (11)$$

where N_{bs} is the number of battery stations for two BEVs and $E1$bs is the energy capacity of one station battery. So, there are two BESSs where each one is $(72V - 480Ah)$ in parallel to each other. So, the total number of battery station ($N_{\text{bs-tot}}$) for the overall CS is calculated as follows:

$$N_{\text{bs-tot}} = 5 * N_{bs} = 5 * 1 = 5. \quad (12)$$

The ratings of load and each source (PV and BESS) are shown in Figure 2.

3.4. Component Sizing of DC-DC Converters

3.4.1. Design of Cascaded Buck Converter for PV System. At MPP, the voltage is 126 V. As a result, we must lower it to the prescribed 1% ripple in output voltage and 20% ripple in output current, or the DC-link voltage of 100 V. To get the most power, the first buck converter is employed, and the second one controls the DC-link voltage. As shown in equations (13)–(15), the duty ratio, inductance, and capacitance of each buck converter are as follows:

$$D = \frac{V_o}{V_{\text{in}}}, \quad (13)$$

$$L_{\text{buck}} = \frac{V_o * (V_{\text{in}} - V_o)}{\Delta i_0 F_{\text{sw}} V_{\text{in}}}, \quad (14)$$

$$C_{o-\text{buck}} = \frac{\Delta i_0}{8\Delta V_o F_{\text{sw}}}. \quad (15)$$

3.4.2. Design of Converter for Battery Vehicle and Battery Station. The converter can function as a buck or boost converter, charging or discharging, depending on the battery

mode. The first plug has a voltage level of 72 V for lithium-ion battery vehicles, while the second plug has a voltage level of 48 V for similar lithium-ion battery vehicles. There are two distinct charging plugs/charging ports. As a result, there are two buck regulators for battery vehicles, and V2G is not considered. However, the boost mode occurs during the BESS's discharge, and the boost equations can be used to determine the design elements (L_{in}, C_{in}, C_o) of each converter. The boost equations are displayed below.

$$D = 1 - \frac{V_{\text{in}}}{V_o},$$

$$L_{\text{boost}} = \frac{D V_{\text{in}}}{\Delta i_0 F_{\text{sw}}}, \tag{16}$$

$$C_{o-\text{boost}} = \frac{D i_0}{\Delta V_o F_{\text{sw}}}.$$

The buck-boost converter uses L and C_{o} at their maximum values because it can function in both modes. To lower switching losses, improve overall performance as an efficient converter, and support continuous current operating mode with the inductance value, the switching frequency F_{sw} in this article is 5 kHz. As demonstrated in [40], the peak efficiency decreases when the switching frequency is high. The outcomes based on these laws with standards values are depicted in Table 2 and are indicated by the arrows above.

4. Power Flow and Modes of Operation with Conditions and Constraints

This study presents a suggested power control strategy for a PV charging facility. The system's design consists of several PV panel strings connected to individual DC/DC converters that share a common DC side. The flow of power during each of the CS's five operational modes is depicted in Figure 2.

4.1. Modes of Operation. Figure 4 shows the direction of power flow during five modes of operation of the ICS.

4.1.1. Mode 1: PV Charges EV Battery Only. In this mode, the 10 EVs are charged only from the PV system and the two switches are opened, as shown in Figure 4(a). This mode is chosen when one of the following conditions exists:

$$P_{\text{pv}} \geq P_{v\text{eh}}, \tag{17}$$

$$\text{SOC}_{\text{bs}} \geq \text{SOC}_{\text{bs-max}}, \tag{18}$$

$$P_{v\text{eh}} = P_{\text{Pv}}. \tag{19}$$

4.1.2. Mode 2: Battery Storage Charges EV Battery Only. The photovoltaic system does not produce any power in this mode, as depicted in Figure 4(b), either because of insufficient radiation or unfavorable weather. The PV's DC/DC buck converter is separated, and the BS only uses a buck-boost converter in the discharging mode to supply the power needed to charge the EVs. The battery station side DC/DC buck-boost converter controls the output voltage to charge the EVs. The BESS keeps supplying power until the EVs are fully charged because that is how it is intended to charge them. In the figure, one switch is open while the other is closed. When one of the circumstances listed below, as in equations (20)–(22), is true, this mode is selected.

Table 2: Converter specifications.

Converter	F_{sw} (kHz)	L (μH)	C_o (μF)
Buck-boost of EVs and BS (100 V–72 V)	5	1500	1000
Buck-boost of EVs (100 V–48 V)		2400	2200
Cascaded buck converter (126 V–100 V)		510	2200

$$P_{\text{bs}} \geq P_{\text{Pv}}, \tag{20}$$

$$\text{SOC}_{\text{bs}} \geq \text{SOC}_{\text{bs-min}}, \tag{21}$$

$$P_{v\text{eh}} = P_{\text{bs-avilable}}. \tag{22}$$

4.1.3. Mode 3: PV Charges BESS Only. As indicated in Figure 4(c), the RB-EMS will select this mode if one of the following requirements is met as in equations (23)–(25). In Figure 4(c), one switch is open while the other is closed.

$$\text{SOC}_{v\text{eh}} = 90\%, \tag{23}$$

$$\text{SOC}_{\text{bs}} < \text{SOC}_{\text{bs-max}}, \tag{24}$$

$$P_{\text{bs}} \leq P_{\text{pv}}. \tag{25}$$

4.1.4. Mode 4: PV Charges BESS and EVs. This mode, in which the PV charges the BESS and BEVs under light load, is depicted in Figure 4(d). Its actions and circumstances are described by equations (26)–(28). In Figure 4(d), one switch is open while the other is closed.

$$P_{v\text{eh}} < P_{\text{pv}}, \tag{26}$$

$$\text{SOC}_{\text{bs}} < \text{SOC}_{\text{bs-max}}, \tag{27}$$

$$P_{\text{bs}} = P_{\text{pv}} - P_{v\text{eh-rated}}. \tag{28}$$

4.1.5. Mode 5: PV and Battery Storage Charge EVs. As seen in Figure 4(e), in this mode, the power produced by the photovoltaic system is less than the electricity needed to charge the EV's battery. While the BESS meets peak load demand, the PV system keeps charging the BEV. The criteria for this mode are summarized in equations (29)–(31). In Figure 4(e), one switch is open while the other is closed.

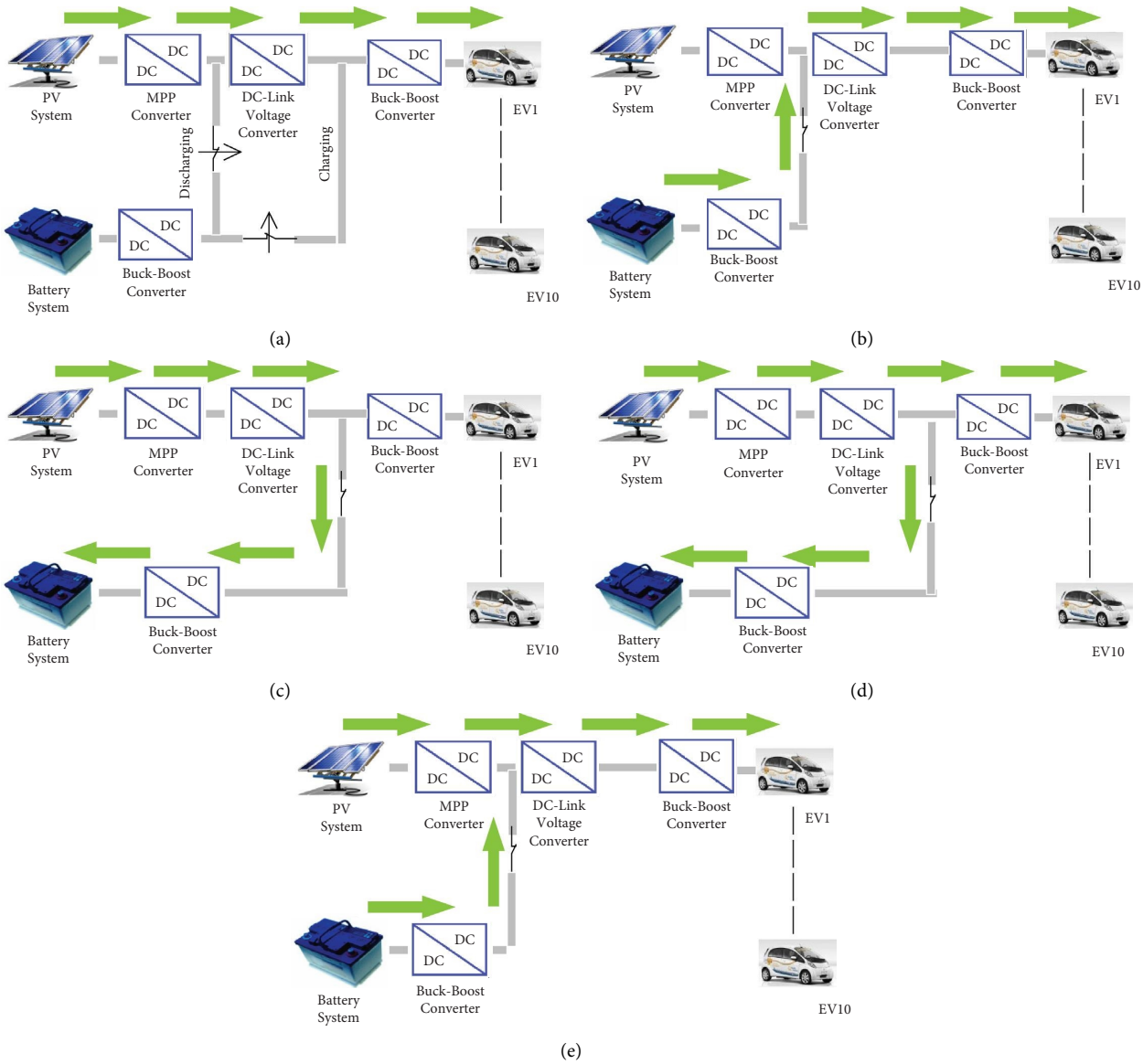

Figure 4: The five modes of operation of the charging station are described as follows: (a) mode 1 (PV charges EVs), (b) mode 2 (SBESS charges EVs), (c) mode 3 (PV charges SBESS), (d) mode 4 (PV charges both EVs and SBESS), and (e) mode 5 (both PV and SBESS charge multiple EVs).

$$P_{\text{veh}} > P_{\text{pv}}, \tag{29}$$

$$\text{SOC}_{\text{bs}} > \text{SOC}_{\text{bs-min}}, \tag{30}$$

$$P_{\text{bs}} = P_{\text{veh}} - P_{\text{pv}}. \tag{31}$$

Table 3 lists the constraints that should be considered to guarantee the continuity of the station.

4.2. Control of DC/DC Buck-Boost Converters

4.2.1. Controls of a Plug-In Charger. The controller of BS in discharging mode is offered in another subsection, but this controller is exclusively for BVs and BS in charging mode, which the V2G does not consider. When the battery is fully charged, there is a decline in battery terminal voltage due to removable battery internal voltage drop, as shown in Figure 5. The PHEV/BEV battery systems typically charge through two stages of operation: the CC mode and the CV mode. The switching point for the charging mode is controlled by the charging termination voltage sent by the battery system controller as shown in Figures 6(c) and 6(d). As shown in Figure 5(a), the charging current for a 72 V battery in the CC mode is 48 A for a 5-hour charging period, whereas in the CV mode, the charging termination voltage is 74 V. Additionally, the charging current for a 48 V battery in the CC mode is 30 A for a 5-hour charging period, while in the CV mode, the charging termination voltage is 50.5 V, as shown in Figure 5(b).

Table 3: System constraints.

Mode	Function	Constraints
Mode#1	PV charges BEVs	(i) P_{pv} is sufficient (ii) $P_{bv} <= P_{pv}$
Mode#2	BS charges BEVs	(i) P_{pv} is not sufficient (ii) BS is available (iii) $P_{bv} <= P_{bs}$
Mode#3	PV charges BS	(i) P_{pv} is sufficient (ii) BEVs are fully charged (no load) (iii) $P_{bs} <= P_{pv}$
Mode#4	PV charges BS and BEVs	(i) P_{pv} is sufficient (ii) Most of BEVs are fully charged (light load) (iii) $P_{bv} + P_{bs<=}P_{pv}$
Mode#5	PV and BS charge BEVs	(i) P_{pv} is sufficient and P_{bs} helps the PV (ii) BEVs are not fully charged (iii) $P_{bv} <= (P_{pv+}P_{bs})$

P_{pv} is the PV power, P_{bv} is the battery vehicle power, and P_{bs} is the battery station power.

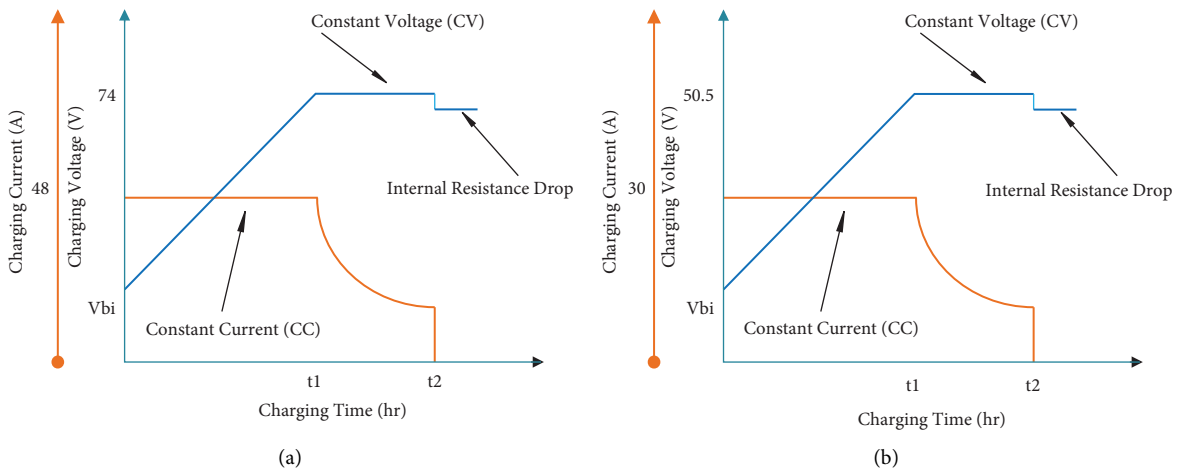

Figure 5: Proposed CCCV charging profile for (a) 72 V vehicle battery and (b) 48 V vehicle battery.

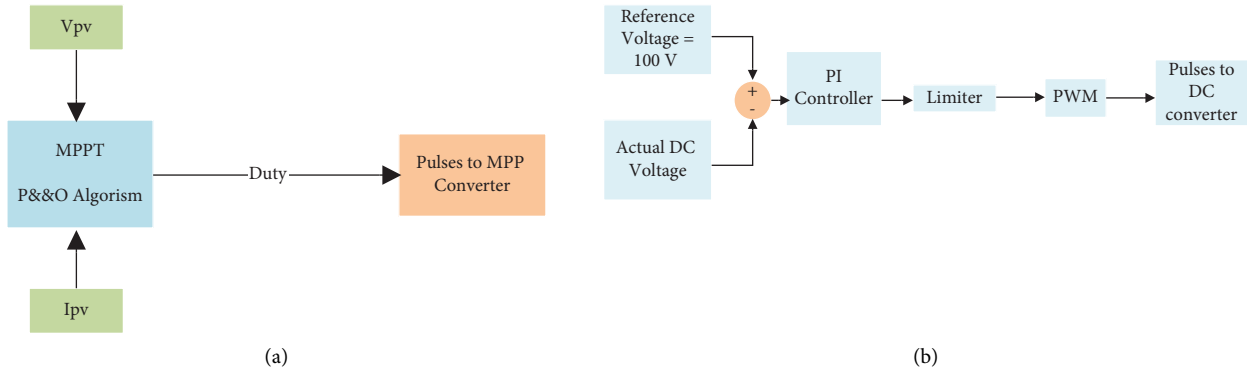

Figure 6: Continued.

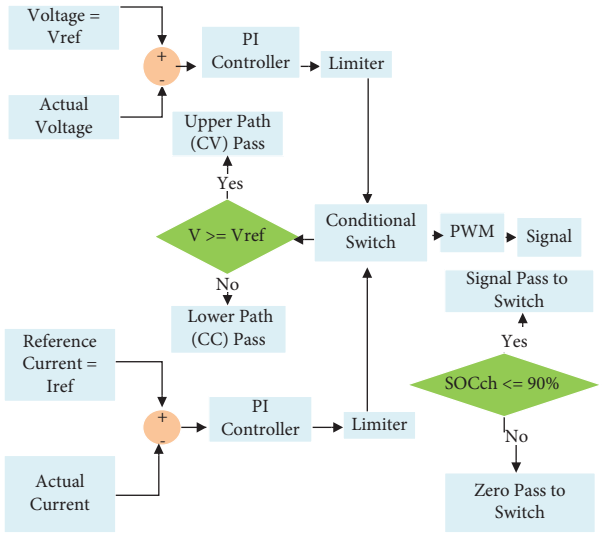

(c)

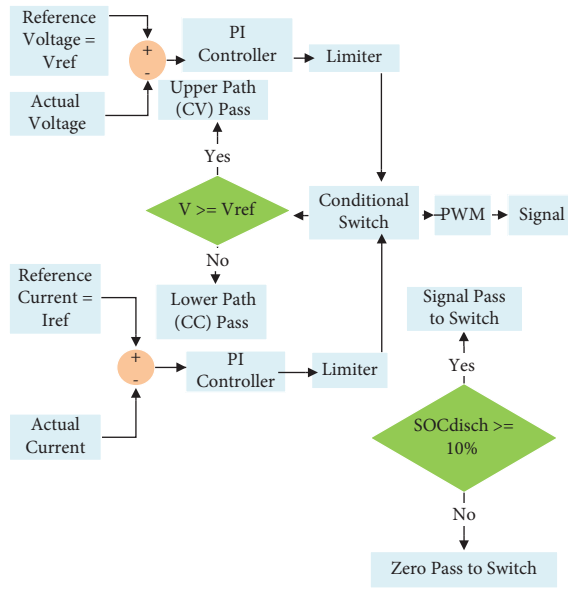

(d)

Figure 6: The four block diagrams of controllers of charging station are as follows: (a) MPP controller, (b) DC-link voltage controller, (c) block diagram of controller for charging battery, and (d) controller block diagram for discharging BS.

The charging control method typically consists of two independent loops, a voltage loop, and a current loop, to implement CC and CV operation. The voltage loop is positioned as an upper loop, which the PI controller generates when the condition is terminated (voltage reaches 74 V), and the lower loop is based on the difference between the desired charging current and the actual battery current as shown in Figure 6(c), which illustrates a typical charging control scheme. For limiting the generated voltage reference and current, the PI controller works in tandem with a saturation block. The desired battery-charging curve with satisfied condition is obtained by feeding the difference between the desired current and the actual charging current to the PI controller in the current loop. The PI controller then uses this information to generate a PWM signal to turn the corresponding power switches on or off.

A charging technique that uses CC first and then CV is suggested based on the CV control method. This approach is an enhanced variant meant to address issues with CV charging, namely, battery damage. The battery is charged using this enhanced approach at a specific CC, and when the battery voltage reaches a specific voltage value, the battery is charged using a CV. When the battery can handle large currents, this upgraded approach assures quick charging with CC, and it also ensures CV charging when the voltage is high and significant polarization is present, leading the charging current to progressively drop. However, the CC and CV values are crucial since they both have the potential to impact the battery's safety and lifespan.

4.2.2. MPP Converter for PV. In order to make the system operate effectively, the PV modules' maximum power is harvested in this process by applying the P&O algorithm to the PV voltage, current, duty ratio, beginning value, maximum ratio, and minimum ratio. As shown in Figure 6(a), an algorithm's output is a duty signal that is applied to the PV's buck converter switch.

4.2.3. DC-Link Voltage Regulation Converter. By comparing the reference voltage to the real DC-link voltage and controlling the error with PI, the DC-link voltage is here regulated to 100 V. As indicated in Figure 6(b), the output of PI is applied to a limiter, which then takes the output of this action from a PWM generator and outputs it to a DC switch.

4.2.4. BS in Discharging Mode. When the BS is operating in boosting mode, power from the BESS (72 V) flows to the DC (100 V). In the upper loop, the reference voltage (72 V) and the actual BS voltage are compared. The error is then applied to the saturation block to limit the control signal that is controlled by PI. However, in the lower loop, the input of PI is error signal that is obtained from comparing the actual current with the reference current (72 A). The control signal is then applied to limiter for the actual current to not exceed the limiting value as shown in Figure 6(d).

5. Simulation Results and Performance Assessments

5.1. Characteristics Validation and Limitations of Power Plant. Table 4 gives a list of the PV's simulation ratings and settings (datasheet with actual figures for the PV model that was used in our project, including testing where 56 PV modules were utilized for each pair of 72 V and 48 V batteries). Tables 5–8 contain information about the battery specifications based on simulations of the MATLAB LiFePO4 3.3v 1.1ah cell.

Battery electric cars (BEVs) are charged using constant current/constant voltage (CCCV) and control voltage and SOC to prevent overcharging and deep discharging because battery voltage is dependent on SOC. Consider the effects of initial and end SOC as well so that the battery is always in a safe range.

5.2. Dynamic Performance of the Power Plants

5.2.1. Mode 1: "PV Charges Vehicles' Batteries". The station battery is out of commission due to the mode state, as indicated in Figures 7(a) and 7(b), and the ten vehicle batteries begin charging from SOCs of 40% to 90% for 72 V vehicle batteries and for 48 V vehicle batteries, respectively. As depicted in Figure 8, the voltage of a 72 V car battery grows to 90% of its SOC when it is in charging mode (74 V). As seen in Figures 8 and 9, in CC mode, only the five 72 V vehicle batteries achieve the setting value of 74 V, causing the vehicle batteries to draw the setting-limited current of 48 A. Once the control reaches the termination condition at 90% of SOC, the CV mode begins. The voltage of the car battery restores to its nominal value in the off-charging mode since the internal resistance's voltage drop is eliminated. The current changes back to 0 A. As seen in Figures 10 and 11, five 48 V battery cars work similarly to five 72 V battery vehicles in that they begin in the CC mode (30 A) and run until they reach the maximum voltage of 50.5 V, at which point they switch to the CV mode, and so on.

According to Figure 12, when the ten vehicle batteries are in charging mode, the output current of the PV is initially at its maximum value (peak period). Then, after two batteries are fully charged at about 0.7 hours, the current slightly decreases and the PV voltage rises. At 1.2 hours, another two batteries are fully charged, and so on. In the off-charging mode, the current drops to 0 A and the PV voltage returns to the open circuit value of 164 V. As seen in Figure 13, the DC voltage increases somewhat during the off time while remaining constant at 100 V during the on period. At full charging, as depicted in Figure 14, the PV and vehicle battery's power changes are equal. Due to some of the vehicle batteries being fully charged, the power generated by the PV is reducing and charging mode is off. PV power and load power are both 0. This mode's efficiency at peak load is roughly 88.54% after one hour.

5.2.2. Mode 2: "Station Battery Charges Vehicle Battery". The ten vehicle batteries start charging from SOCs of 40% to 90% for 72 V vehicle batteries and for 48 V vehicle batteries, respectively, as shown in Figures 15(a) and 15(b), logically validating the design. The station batteries' SOC decreases because they are in discharging mode, as highlighted in Figure 15(c). The PV is out of service due to the mode condition. The charging rate for battery vehicles in CC mode is constant until they enter CV mode, as shown in Figures 16–19, where it changes. As can be seen in Figures 20 and 21, the station battery discharges in CC mode because it does not go beyond any set parameters and does not achieve the termination condition (Vs ≤ 72 V). Eventually, the voltage drops to its present SOC due to the positive discharging current and voltage drop. As depicted in Figure 22, the DC voltage increases somewhat when the charging system is turned off while remaining constant at 100 V

Table 4: The datasheet of the PV module.

Voltage at P_{max}	126 V
Current at V_{max}	0.95 A
Open circuit voltage (V_{oc})	164 V
Short circuit current (I_{sc})	1.17 A
Reference irradiation	1000 W/m^2
Reference temperature	25°C
Maximum power (P_{max})	120 W

Table 5: Battery cell specification.

Nominal voltage	3.3 V
Nominal capacity	1.1 Ah
Operation temperature range	−20 C–+40°C
Fast charge current	4 A
Charging voltage	3.6 V
Max continuous discharge current	10 A
Cut of voltage	3.6 to 2 V

Table 6: 72 V vehicle battery specification.

No. of parallel cells	219
No. of series cells	22
Nominal voltage	72 V
Nominal capacity	240 Ah
Operation temperature range	−20–+40°C
Charging current	48 A (0.2°C)
Charging voltage	74
Cut of voltage	80 to 44 V
Max. continuous discharge current	480 A (2°C)

Table 7: 48 V vehicle battery specification.

No. of parallel cells	137
No. of series cells	15
Nominal voltage	48 V
Nominal capacity	150 Ah
Operation temperature range	−20 to +40°C
Charging current	30 A (0.2°C)
Charging voltage	50.5 V
Cut of voltage	54 to 30 V

Table 8: 72 V station battery specification.

No. of parallel cells	437
No. of series cells	22
Nominal voltage	72 V
Nominal capacity	480 Ah
Operation temperature range	−20–+40°C
Charging current	48 A (0.2°C)
Charging voltage	74
Cut of voltage	80 to 44 V
Max. continuous discharge current	960 A (2°C)

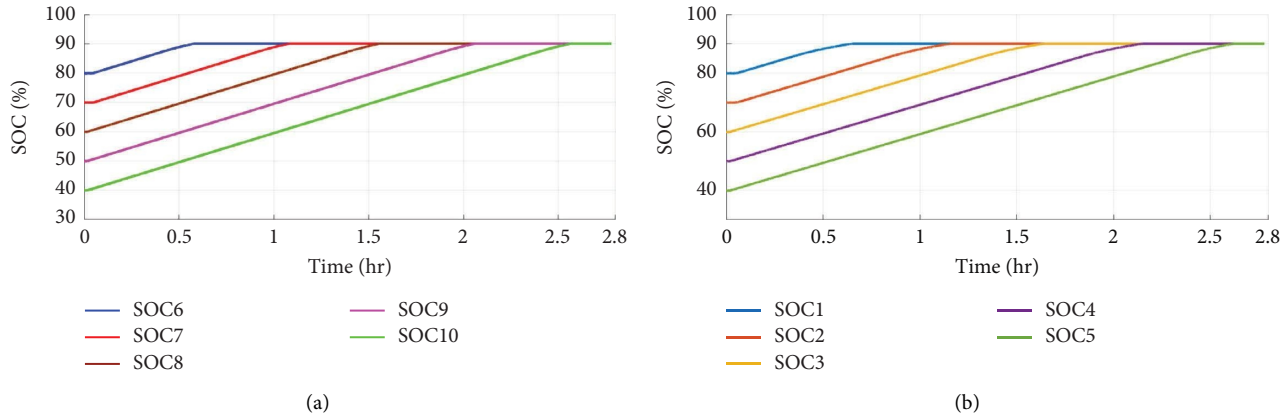

Figure 7: SOCs of battery vehicles: (a) for 72 V battery and (b) for 48 V battery.

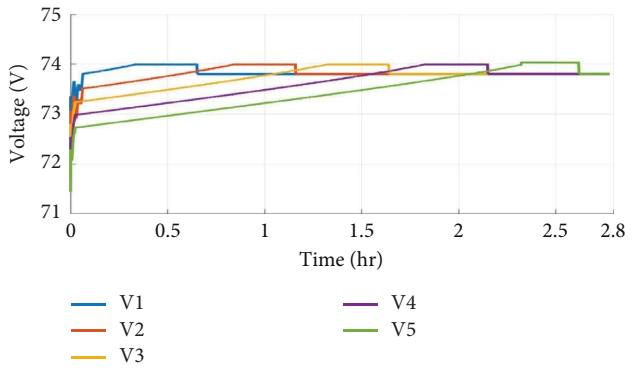

Figure 8: Voltage of vehicle battery of 72 V.

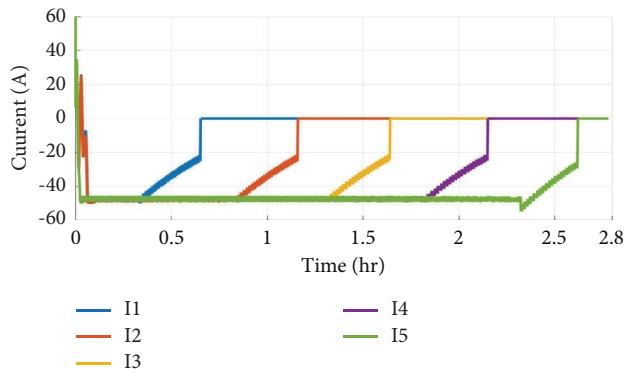

Figure 9: Current of vehicle battery of 72 V.

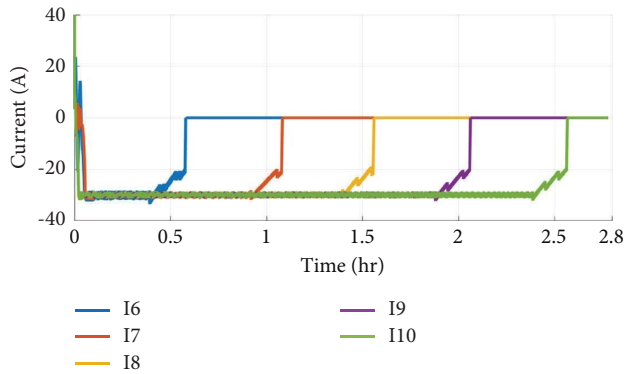

Figure 10: Current of vehicle battery of 48 V.

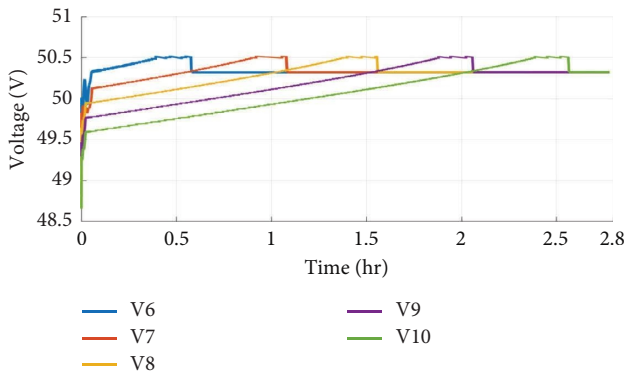

Figure 11: Voltage of vehicle battery of 48 V.

during charging. Figure 23 illustrates this in charging mode. Vehicle batteries and station batteries both experience power fluctuations. As the SOC of the battery rises, the power supplied by the BS decreases. BESS and BEV power is zero in off-charging mode. This mode's efficiency at peak load is roughly 89.61% at 1 hour.

5.2.3. Mode 3: "PV Charges Station Battery". According to Figure 24, the station battery begins charging at the lowest value (64%) and continues until the SOC reaches 90%. The voltage and current of station batteries are under CCCV control, as shown in Figures 25 and 26, where the current is constant until the voltage reaches a specific value of 74 V, at which point it enters CV mode until it is fully charged. The CV period of the station battery pack is very short because it has a capacity that is twice that of the vehicle battery, despite the fact that they have the same voltage. As depicted in Figure 27, the PV's voltage and current are constant during the on period of charging until the batteries are fully charged one after the other. At this point, the voltage increases slightly, the current decreases in relation to the voltage, and at the off period, the voltage rises to no-load voltage (164 V).

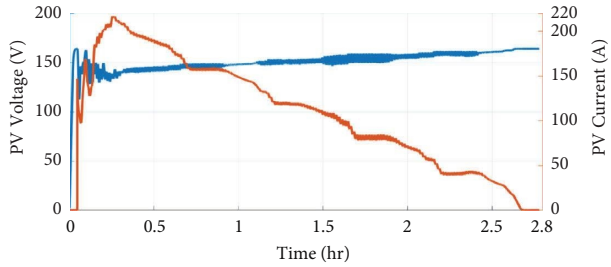

Figure 12: Voltage and current of PV.

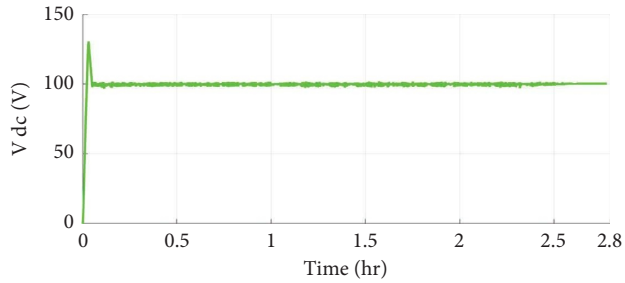

Figure 13: Voltage of DC link.

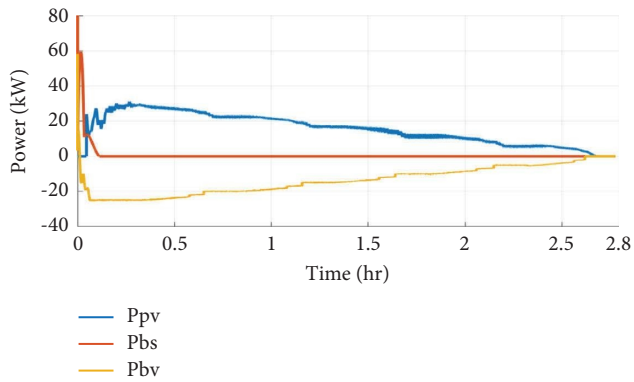

Figure 14: Power of PV and vehicle battery.

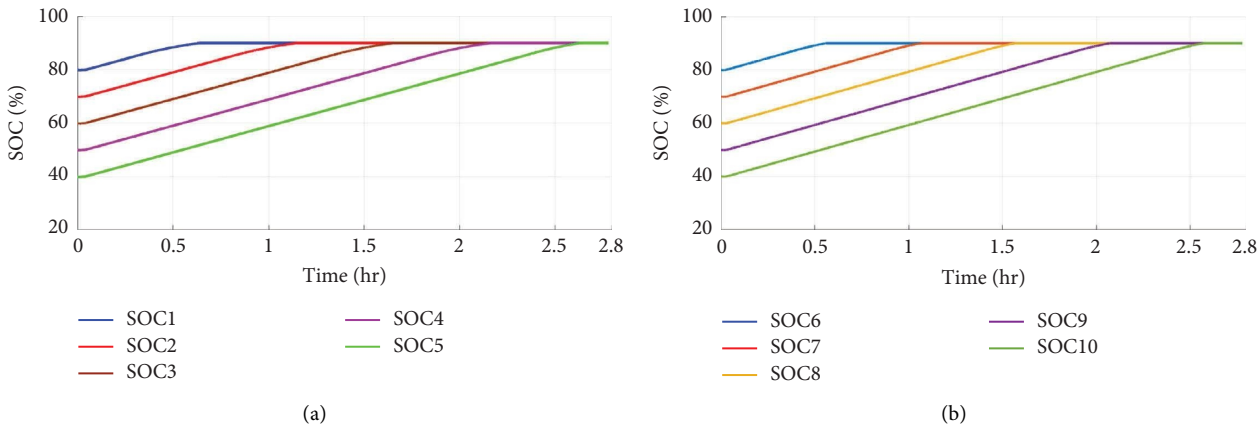

Figure 15: Continued.

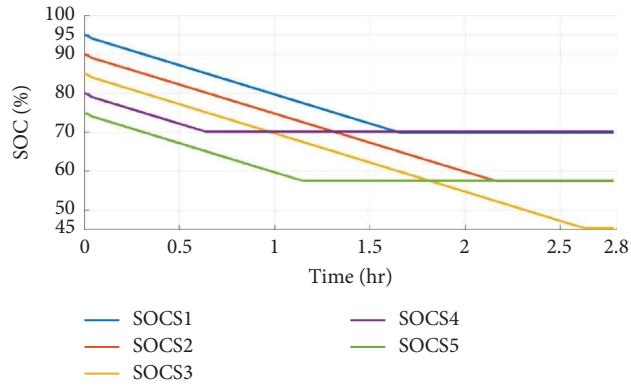

(c)

Figure 15: SOCs of all batteries: (a) for 72 V battery vehicle, (b) for 48 V battery vehicle, and (c) for 72 V battery station.

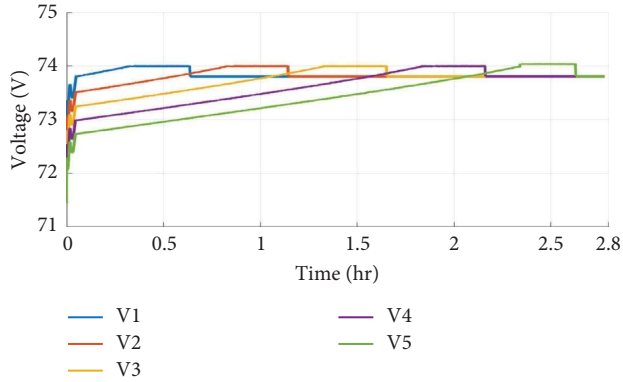

Figure 16: Voltage of vehicle battery of 72 V.

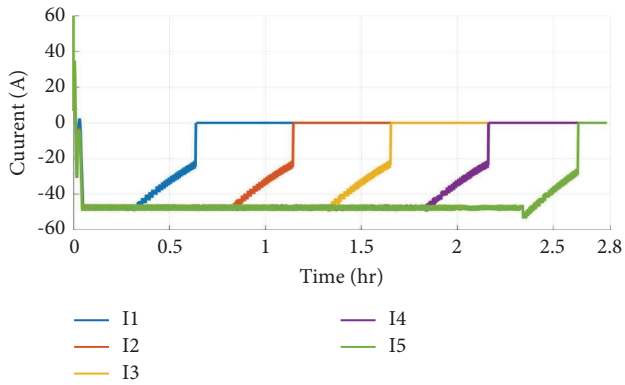

Figure 17: Current of vehicle battery of 72 V.

As depicted in Figure 28, during the charging phase, the DC voltage remains constant at 100 V, the reference voltage, and during the discharging phase, the voltage slightly exceeds its reference voltage (100 V). As seen in Figure 29, the station battery receives the power from the PV system as a result for this mode's conditions and constraints. This mode's efficiency at peak load is roughly 86.86% at 1 hour.

5.2.4. Mode 4: "PV Charges Station and Vehicle Battery". When there is little load, the PV can charge the battery pack at the station during the sun's peak hours. The vehicle batteries charge from their lowest values to their highest values before stopping, as shown in Figures 30(a) and 30(b), whereas the station batteries charge similarly but with a different initial SOC. The five battery vehicles draw

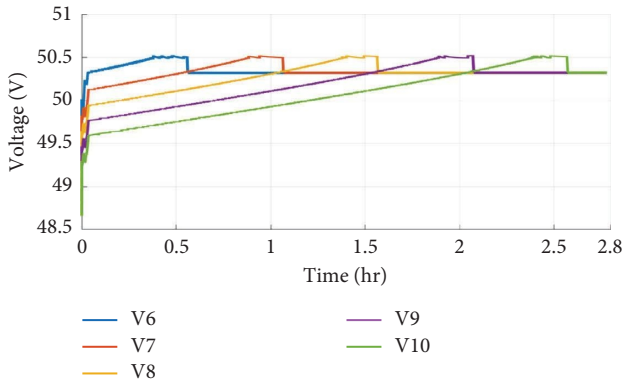

Figure 18: Voltage of vehicle battery of 48 V.

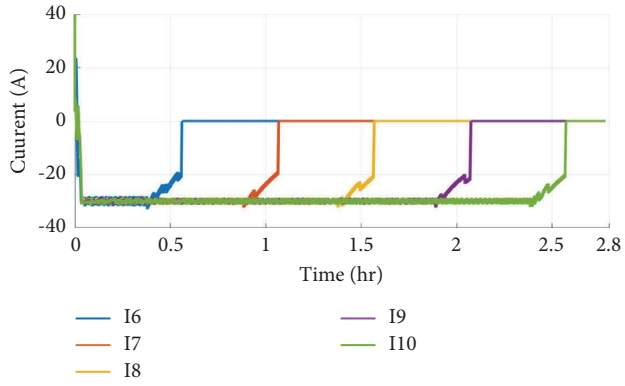

Figure 19: Current of vehicle battery of 48 V.

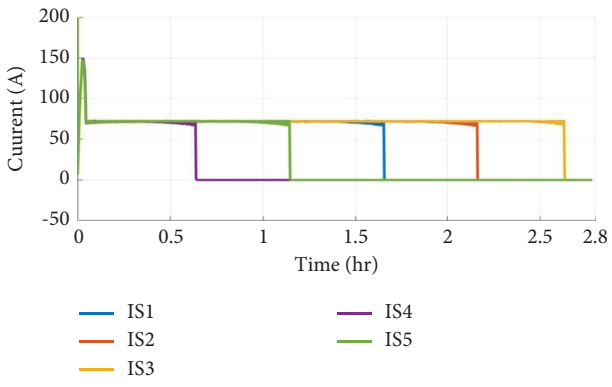

Figure 20: Current of station battery.

the set-limit current as shown is constant in CC mode because the battery is not reach to the set-limit voltage, and the five battery vehicles enter CV mode after 50.5 V of battery vehicle as shown in Figures 31 and 32. This happens when the voltage of the five vehicle batteries increases to 90% of their SOC. The vehicle voltage and current in the preceding two figures, Figures 33 and 34, which start in CC mode then enter the CV mode after reaching the limited voltage and so on, are similar to the station battery voltage and current in Figures 26 and 27. Because the voltage drop

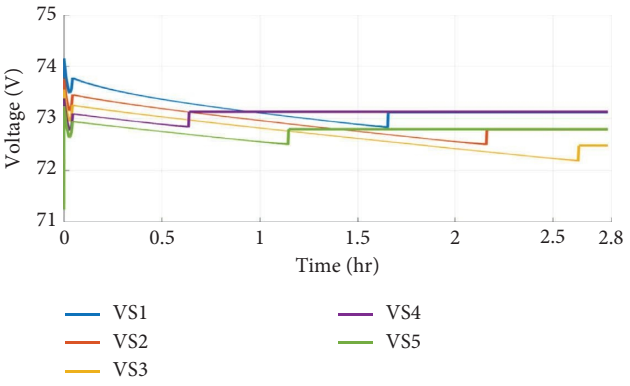

Figure 21: Voltage of station battery.

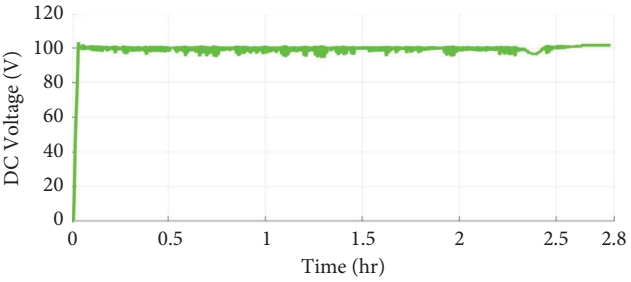

Figure 22: Voltage of DC link.

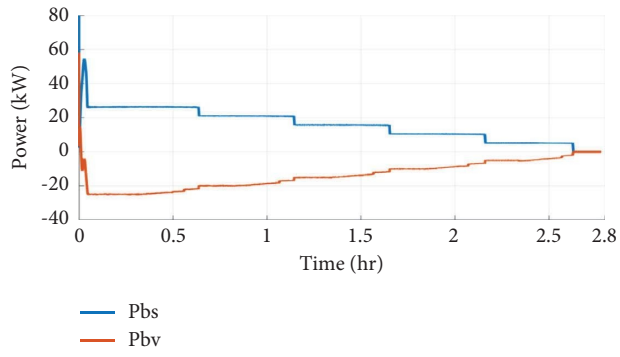

Figure 23: Power of station and vehicle battery.

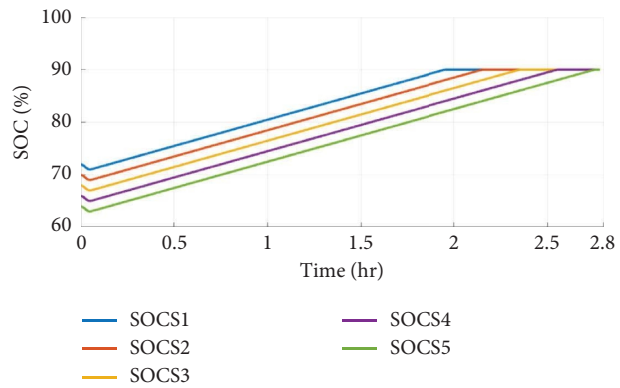

Figure 24: SOC of station battery.

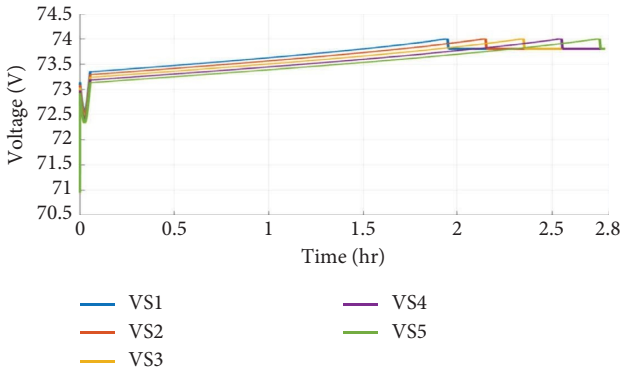

Figure 25: Voltage of station battery.

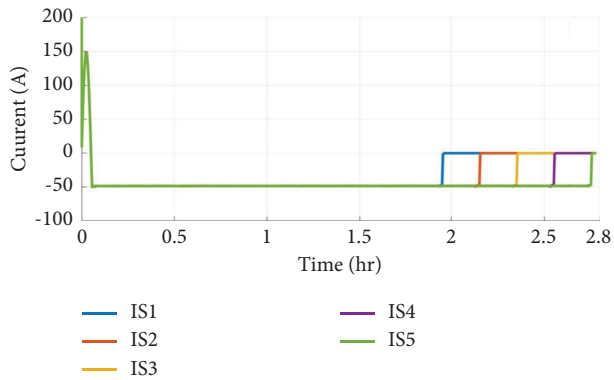

Figure 26: Current of station battery.

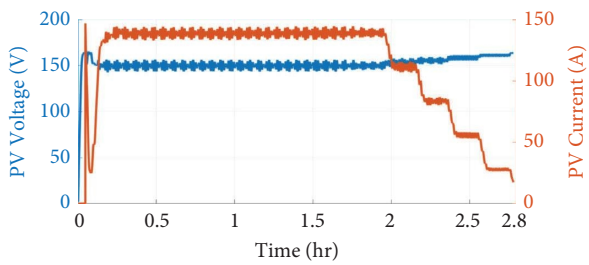

Figure 27: Voltage and current of PV.

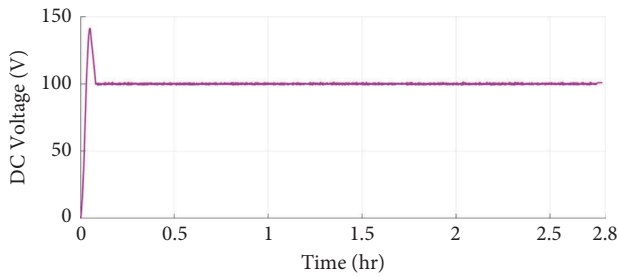

Figure 28: Voltage of DC link.

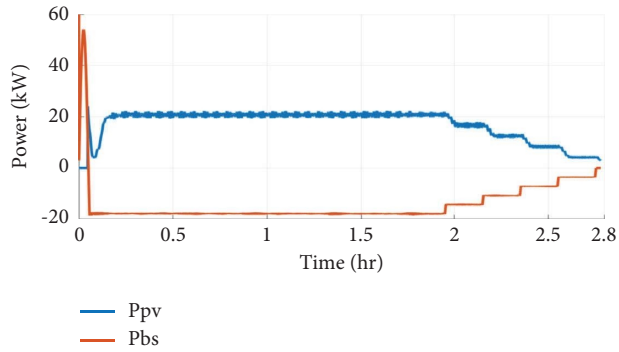

Figure 29: PV and station power.

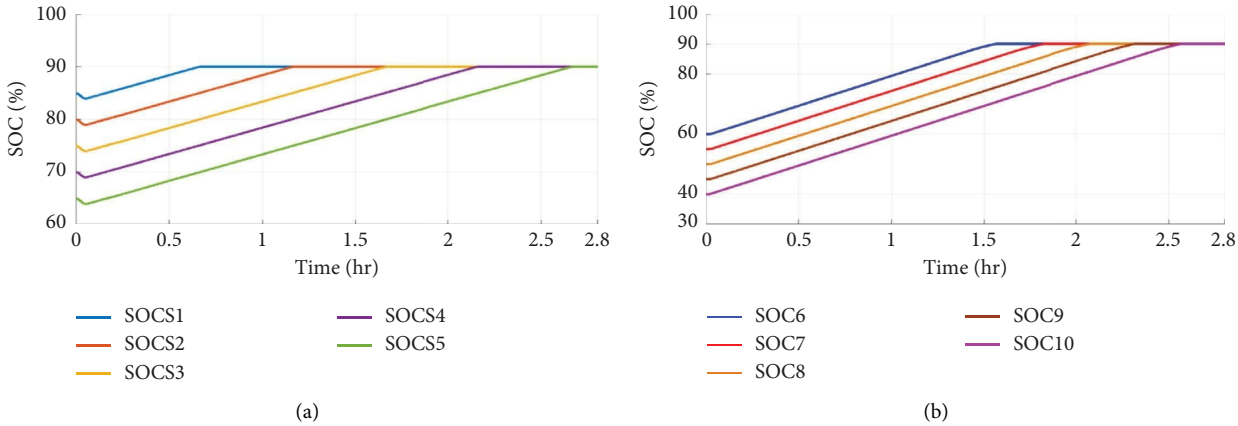

Figure 30: SOC of batteries: (a) for station batteries and (b) for vehicle battery.

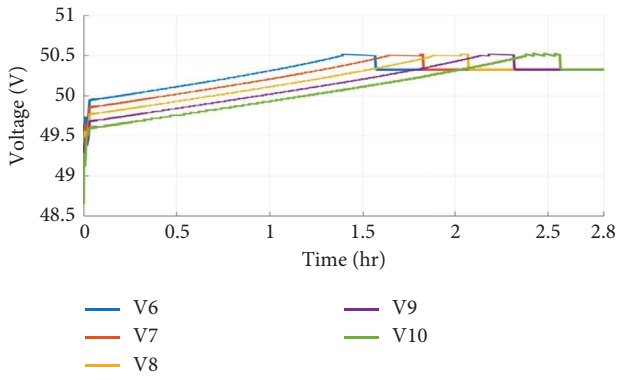

Figure 31: Voltage of vehicle of 48 V.

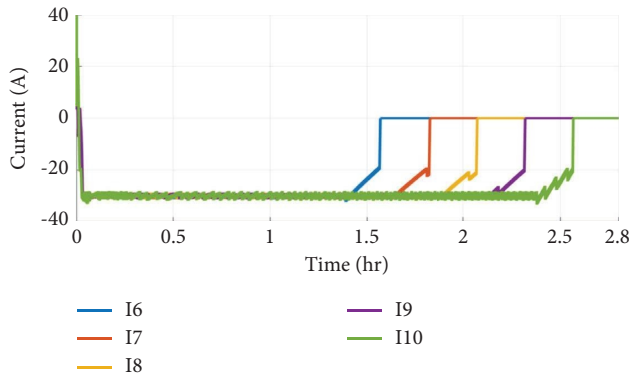

Figure 32: Current of vehicle of 48 V.

on the internal resistance is removed and the current is zero in the off-charging mode, the voltage of the vehicle battery and the station battery lowers. As depicted in Figure 35, a significant current is initially needed to charge the batteries, and thus the PV operates at MPP. Next, the PV voltage is increased gradually, and the current remains constant while dropping, until the vehicle battery achieves its full capacity. A DC link is illustrated in Figure 36; voltage is at a constant value (100 V for the reference value). The effect of a heavy load is depicted in the first curve, which causes a drop in voltage. As can be seen in Figure 37, as soon as the station battery and vehicle battery SOCs are fully charged, the PV power starts to decline and eventually reaches zero. At one hour, this mode's efficiency is around 89.52%.

5.2.5. Mode 5: "PV and Station Battery Charge Vehicle Batteries". The SOC of car batteries rises during charging from a minimum value of 40% to a maximum value of 90%, as shown in Figures 38(a)–38(c). When two BVs are fully

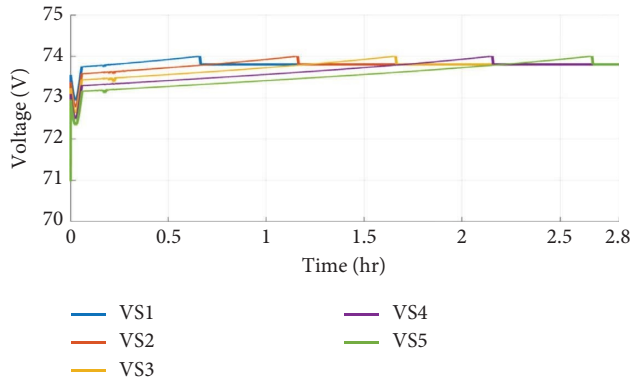

Figure 33: Voltage of station battery.

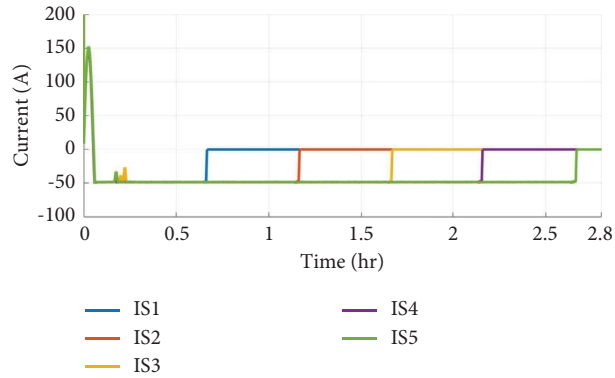

Figure 34: Current of station battery.

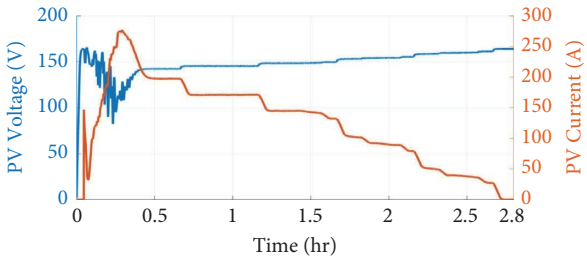

Figure 35: Voltage and current of PV.

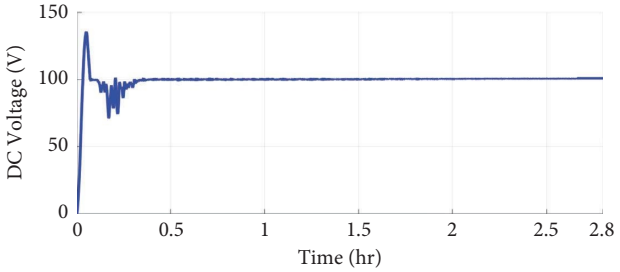

Figure 36: Voltage of DC link.

charged, one of BESS is removed from them until the vehicle batteries reach their maximum value of 90%, and SOC of station batteries drops to various values.

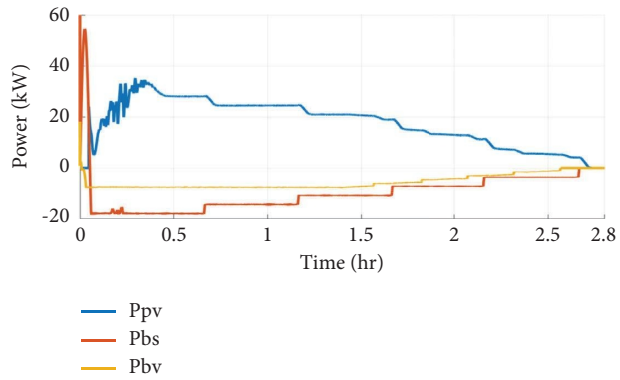

Figure 37: Power of PV, station battery, and vehicle battery.

As seen in Figures 39 and 40, the voltage of the car batteries increases to 90% of their SOC, or 74 V and 50.5 V, respectively, while the charging mode is activated. The car batteries initially draw the rated current during charging because their voltages (74 V and 48 V, respectively) do not exceed the limited voltage. The current then steadily drops with constant voltage (CV), as illustrated in Figures 41 and 42. Just when the car batteries reach their maximum SOC, the voltage of the battery recovers to its nominal value in the off-charging state because the voltage drop on the internal resistance is eliminated and the current drops to 0 A. As seen

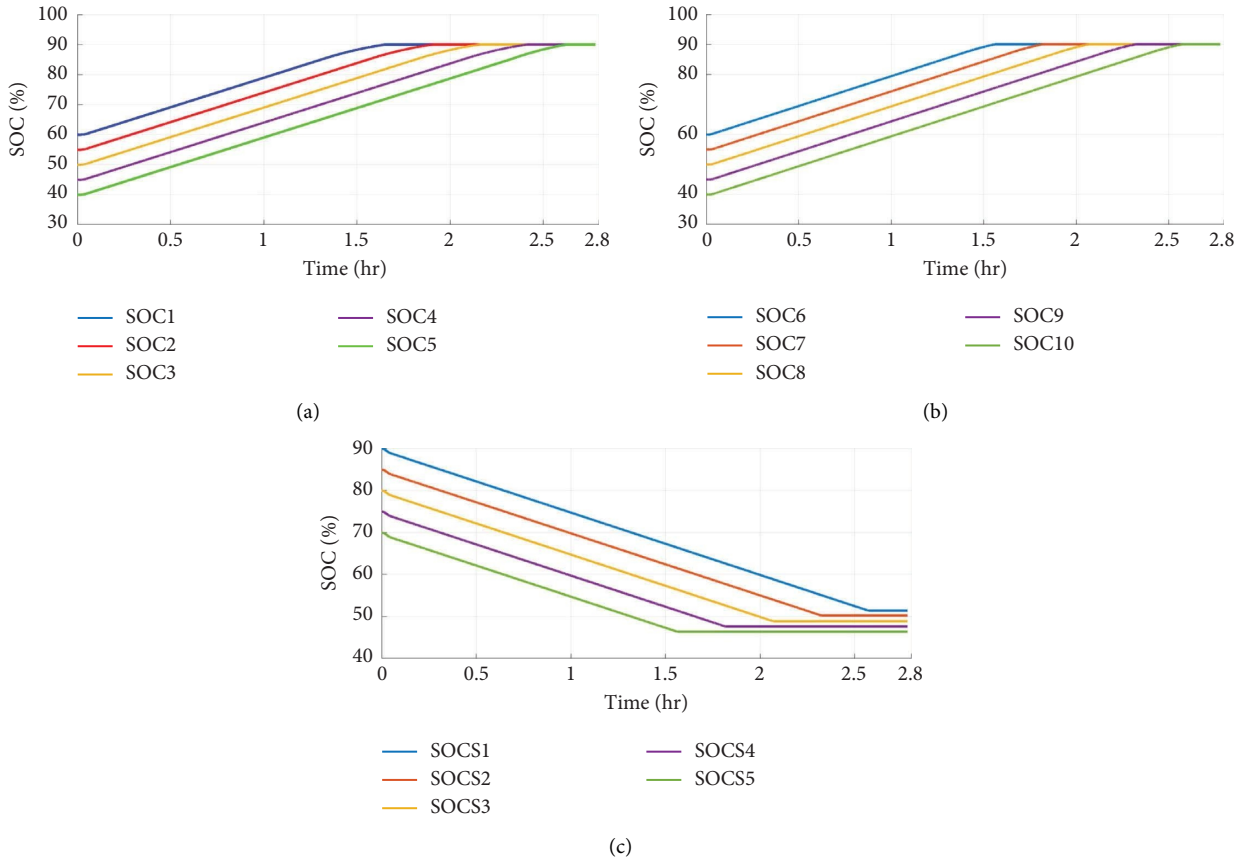

Figure 38: SOCs of all batteries: (a) for 72 V battery vehicle, (b) for 48 V battery vehicle, and (c) for 72 V battery station.

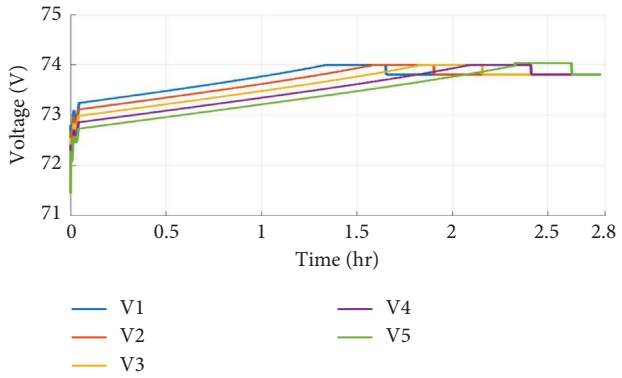

Figure 39: Voltage of vehicle battery of 72 V.

in Figures 43 and 44, station batteries' voltage decreases over time while maintaining a constant output current because they participate in photovoltaics (PV) as a backup source. In the off mode, however, the voltage rises to a higher value due to the removal of internal resistance, but the current is reduced to zero. According to Figure 45, in the on-charging mode, the PV's output current increases slightly at first, which causes the output voltage to drop; over time, the

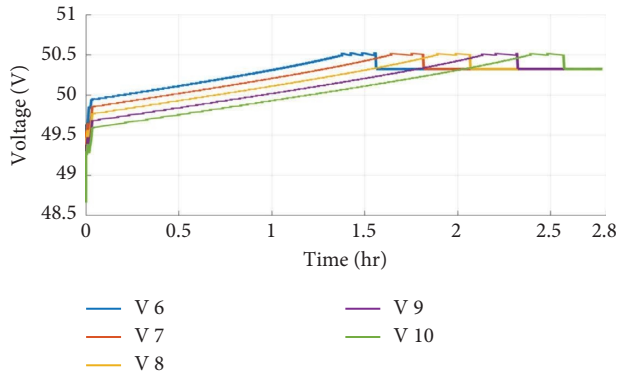

Figure 40: Voltage of vehicle battery of 48 V.

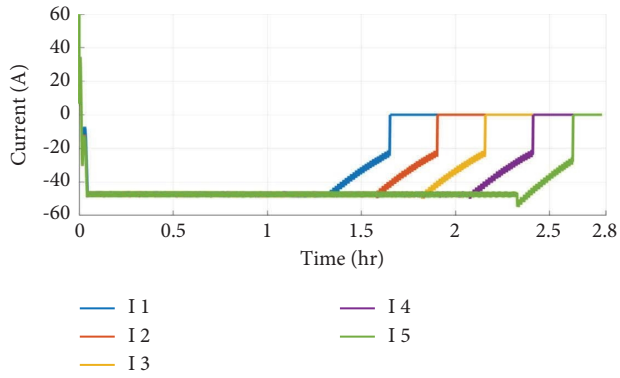

Figure 41: Current of vehicle battery of 72 V.

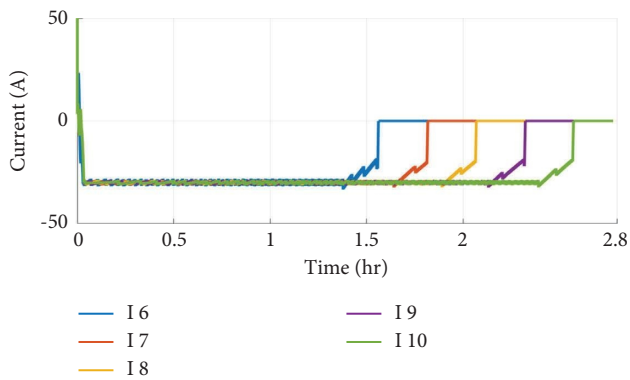

Figure 42: Current of vehicle battery of 48 V.

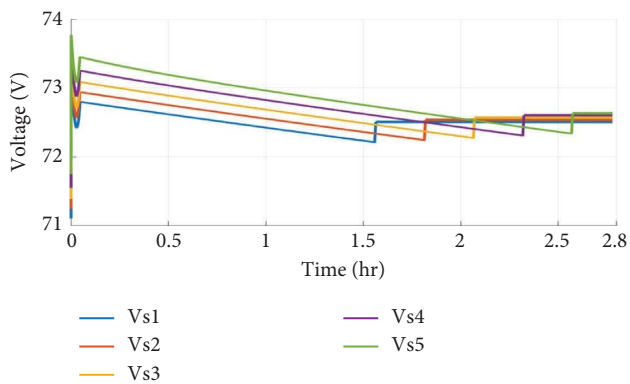

Figure 43: Voltage of station battery.

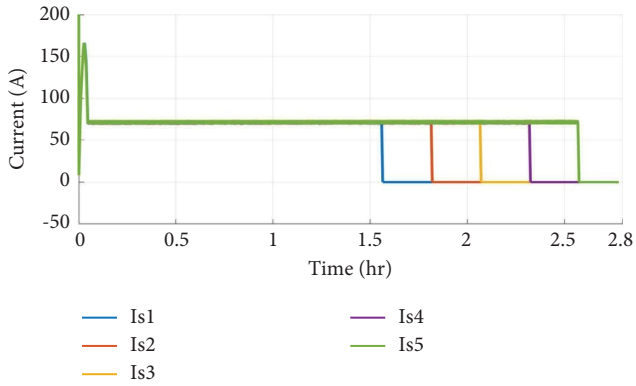

Figure 44: Current of station battery.

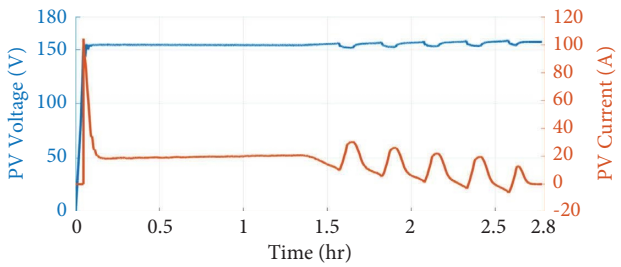

Figure 45: Voltage and current of PV.

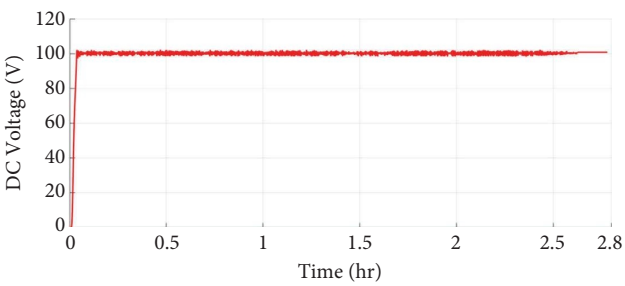

Figure 46: Voltage of DC link.

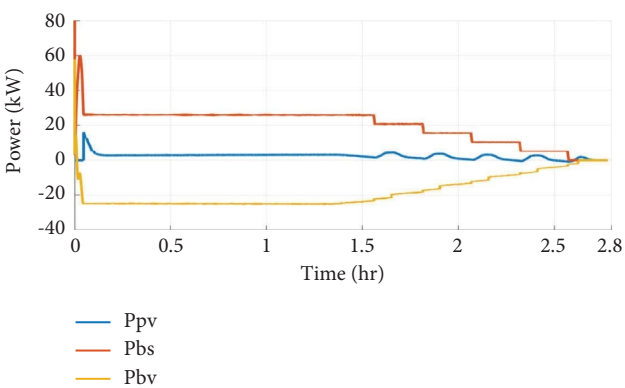

Figure 47: Power of PV, station battery, and vehicle battery.

Table 9: Efficiency calculation.

Mode	Input power	Output power	Efficiency (η)
Mode#1	$P_{\text{in}} = P_{\text{pv}}$	$P_o = \sum_{i=0}^{10} P_{\text{bvi}}$	88.54%
Mode#2	$P_{\text{in}} = \sum_{x=0}^{5} p_{\text{bsx}}$	$P_o = \sum_{i=0}^{10} P_{\text{bvi}}$	89.61%
Mode#3	$P_{\text{in}} = P_{\text{pv}}$	$P_o = \sum_{x=0}^{5} p_{\text{bsx}}$	86.86%
Mode#4	$P_{\text{in}} = P_{\text{pv}}$	$P_o = \sum_{x=0}^{5} p_{\text{bsx}} + \sum_{i=0}^{10} P_{\text{bvi}}$	89.52%.
Mode#5	$P_{\text{in}} = P_{\text{pv}} + \sum_{x=0}^{5} p_{\text{bsx}}$	$P_o = \sum_{i=0}^{10} P_{\text{bvi}}$	86.84%

P_{pv} is the power of PV as primary source, p_{bv} is battery vehicle power as load, and p_{bs} is the battery station power as backup source.

voltage rises until the vehicle battery reaches 90% of its SOC; in the off-charging mode, the voltage returns to the open circuit voltage and the current decreases to 0 A. As seen in Figure 46, when the station batteries are working as a source to support the DC voltage, the DC voltage is constant at 100 V and more stable, and when the station batteries are not working as a source, the voltage slightly rises. As seen in Figure 47, the PV power and station battery power are added together to determine how much power is changing in the car battery. Because some of the car batteries' SOC reaches 90% before all are fully charged, the power provided by the PV and station batteries drops until it reaches zero. This mode's efficiency at peak load is roughly 86.84% at 1 hour.

5.2.6. Efficiency Calculation. For each mode, the efficiency can be calculated by dividing the output power (P_o) by the input power P_{in} as highlighted in the following equation:

$$\eta = \frac{P_o}{P_{\text{in}}}. \tag{32}$$

The calculated efficiency for all modes is shown in Table 9.

6. Conclusion

In this research, a rule-based energy management approach for BEVs to manage the power flow in PV/BS-based CS has been developed with the proposed effective flexible cascaded converter to regulate the DC-link voltage and extract the possible maximum power from PV. First, parametric design and parameter selection are discussed in relation to the daily load needs. The suggested system is then validated using appropriate control systems and modes of operation. The simulation results are shown at the conclusion of this study, demonstrating that the second mode is the most effective mode and that the design was correct (station battery charges vehicle battery). The future suggestion for this study is to improve the overall performance by using new control techniques and smooth mode selection.

Data Availability

The data used to support the findings of this study have not been made available.

Conflicts of Interest

The authors declare that they have no conflicts of interest.

References

[1] S. Rajakaruna, "Plug in electric vehicles in smart grids," Springer Charging Strategies, Berlin, Germany, 2015.

[2] P. Garca-Trivino, L. M. Fernandez-Ramirez, J. P. Torreglosa, and F. Jurado, "Control of electric vehicles fast charging station supplied by PV/energy storage system/grid," in *Proceedings of the 2016 IEEE International Energy Conference (ENERGYCON)*, Leuven, Belgium, June 2016.

[3] B. Bendjedia, N. Rizoug, M. Boukhnifer, and F. Bouchafaa, "Intelligent energy management of a multisource power supply for electric vehicle application," in *Proceedings of the 2017 IEEE Vehicle Power and Propulsion Conference (VPPC)*, Belfort, France, December 2018.

[4] C. H. Swetha, N. S. Jayalakshmi, K. M. Bhargavi, and P. B. Nempu, "Control strategies for power management of PV/battery system with electric vehicle," in *Proceedings of the 2019 IEEE International Conference on Distributed Computing, VLSI, Electrical Circuits and Robotics (DISCOVER)*, Manipal, India, August 2019.

[5] A. Verma and B. Singh, "Multimode operation of solar PV array, grid, battery and diesel generator set based EV charging station," *IEEE Transactions on Industry Applications*, vol. 56, no. 5, pp. 5330–5339, 2020.

[6] S. D. C. Lobato, J. H. D. G. Pinto, R. N. D. M. Carneiro, G. F. Avelar, J. A. Valentim, and A. A. Ferreira, "Development of an electric vehicle charging station," *SBSE 2018- 7th Brazilian Electrical Systems Symposium*, vol. 20, pp. 1–6, 2018.

[7] D. Devendra, S. Malkurthi, A. Navnit, and A. M. Hussain, "Compact electric vehicle charging station using open charge point protocol (OCPP) for E-scooters," in *Proceedings of the 2021 International Conference on Sustainable Energy and Future Electric Transportation (SEFET)*, Hyderabad, India, January 2021.

[8] A. K. Kalakanti and S. Rao, "Charging station planning for electric vehicles," *Systems*, vol. 10, no. 1, pp. 6–26, 2022.

[9] F. Ahmad, A. Iqbal, I. Ashraf, M. Marzband, and I. khan, "Optimal location of electric vehicle charging station and its impact on distribution network: a review," *Energy Reports*, vol. 8, pp. 2314–2333, 2022.

[10] A. Danese, B. N. Torsæter, A. Sumper, and M. Garau, "Planning of high-power charging stations for electric vehicles: a review," *Applied Sciences*, vol. 12, no. 7, p. 3214, 2022.

[11] S. Rastgoo, Z. Mahdavi, M. Azimi Nasab, M. Zand, and S. Padmanaban, "Using an intelligent control method for

electric vehicle charging in microgrids," *World Electric Vehicle Journal*, vol. 13, no. 12, p. 222, 2022.

[12] M. Rajabzadeh, S. M. T. Bathaee, and M. A. Golkar, "Advanced DC-link voltage regulation of fuel-cell electric vehicle," *COMPEL: The International Journal for Computation & Mathematics in Electrical & Electronic Engineering*, vol. 35, no. 3, pp. 943–958, 2016.

[13] A. Cabrera-Tobar, N. Blasuttigh, A. Massi Pavan, V. Lughi, G. Petrone, and G. Spagnuolo, "Energy scheduling and performance evaluation of an e-vehicle charging station," *Electronics*, vol. 11, no. 23, pp. 3948–4017, 2022.

[14] A. C. R. Teixeira, J. R. Sodré, and J. Ricardo, "Impacts of replacement of engine powered vehicles by electric vehicles on energy consumption and CO 2 emissions," *Transportation Research Part D: Transport and Environment*, vol. 59, pp. 375–384, 2018.

[15] K. Kouka and L. Krichen, "Energy management strategy of a photovoltaic electric vehicle charging station," in *Proceedings of the 2019 19th International Conference on Sciences and Techniques of Automatic Control and Computer Engineering (STA)*, Sousse, Tunisia, March 2019.

[16] J. Quispe, "Energy management strategy of a renewable energy based electric vehicle," *Energy*, vol. 4, no. 1, pp. 88–100, 2023.

[17] W. Xiong, X. Yu, and Y. Yang, "Energy management strategy of photovoltaic charging station for electric vehicles in commercial area," *IOP Conference Series: Materials Science and Engineering*, vol. 452, no. 3, Article ID 032024, 2018.

[18] K. Mohamed, H. K. Wolde, A. M. S. Al-Farsi, R. Khan, and S. M. S. Alarefi, "Opportunities for an off-grid solar PV assisted electric vehicle charging station," in *Proceedings of the 2020 11th International Renewable Energy Congress (IREC)*, Hammamet, Tunisia, October 2020.

[19] P. Dorin, P. Toma, E. Radu, and C. Marcian, "Renewable energy EV charging station," in *Proceedings 2021 International Aegean Conference on Electrical Machines and Power Electronics, ACEMP 2021 and 2021 International Conference on Optimization of Electrical and Electronic Equipment, OPTIM*, Kifisia, Greece, July 2021.

[20] A. R. Bhatti and Z. Salam, "Photovoltaic (PV) charging of electric vehicle (EV)," *Electrical Engineering Research Colloquium For Electronics, Power, Instrumentation \& Control And Communication (EERC-2013)*, vol. 1, pp. 102-103, 2013.

[21] N. Priyadarshi, M. S. Bhaskar, P. Sanjeevikumar, F. Azam, and B. Khan, "High-power DC-DC converter with proposed HSFNA MPPT for photovoltaic based ultra-fast charging system of electric vehicles," *IET Renewable Power Generation*, vol. 45, pp. 1–13, 2022.

[22] N. Priyadarshi, P. Sanjeevikumar, M. Bhaskar, F. Azam, I. B. M. Taha, and M. G. Hussien, "An adaptive TS-fuzzy model based RBF neural network learning for grid integrated photovoltaic applications," *IET Renewable Power Generation*, vol. 16, no. 14, pp. 3149–3160, 2022.

[23] N. Priyadarshi, S. Padmanaban, M. S. Bhaskar, and B. Khan, "An experimental performance verification of continuous mixed P-norm based adaptive asymmetrical fuzzy logic controller for single stage photovoltaic grid integration," *IET Renewable Power Generation*, vol. 10, pp. 1–11, 2022.

[24] N. Priyadarshi, S. Padmanaban, S. Member, and P. Kiran, "An extensive practical investigation of fpso-based mppt for grid integrated pv system under variable operating conditions with anti-islanding protection," *IEEE Systems Journal*, vol. 13, pp. 1–11, 2018.

[25] N. Priyadarshi, S. Padmanaban, and S. Member, "An experimental estimation of hybrid anfis – pso-based mppt for pv grid integration under fluctuating sun irradiance," *IEEE Systems Journal*, vol. 14, pp. 1–12, 2019.

[26] N. Priyadarshi, S. Padmanaban, S. Member, M. S. Bhaskar, and F. Blaabjerg, "A hybrid photovoltaic-fuel cell-based single-stage grid integration with lyapunov control scheme," *IEEE Systems Journal*, vol. 14, pp. 1–9, 2019.

[27] P. He and A. Khaligh, "Comprehensive analyses and comparison of 1 kW isolated DC-DC converters for bidirectional EV charging systems," *IEEE Transactions on Transportation Electrification*, vol. 3, no. 1, pp. 147–156, 2017.

[28] M. Kerler, P. Burda, M. Baumann, and M. Lienkamp, "A concept of a high-energy, low-voltage ev battery pack," in *Proceedings of the 2014 IEEE International Electric Vehicle Conference*, Florence, Italy, December 2014.

[29] F. Musavi, M. Edington, W. Eberle, and W. G. Dunford, "Evaluation and efficiency comparison of front end AC-DC plug-in hybrid charger topologies," *IEEE Transactions on Smart Grid*, vol. 3, no. 1, pp. 413–421, 2012.

[30] G. Y. Choe, J. S. Kim, B. K. Lee, C. Y. Won, and T. W. Lee, "A Bi-directional battery charger for electric vehicles using photovoltaic PCS systems," in *Proceedings of the 2014 2010 IEEE Vehicle Power and Propulsion Conference*, Lille, France, September 2010.

[31] D. Patil, M. K. McDonough, J. M. Miller, B. Fahimi, and P. T. Balsara, "Wireless power transfer for vehicular applications: overview and challenges," *IEEE Transactions on Transportation Electrification*, vol. 4, no. 1, pp. 3–37, 2018.

[32] A. Nasir, "Design and development of a constant current constant voltage fast battery charger for electric vehicles," in *Proceedings of The 4th International Conference on Modern Research in Science Engineering and Technology*, Berlin, Germany, March 2021.

[33] S. Wang, Y. Liu, and X. Wang, "Resonant converter for battery charging applications with CC/CV output profiles," *IEEE Access*, vol. 8, pp. 54879–54886, 2020.

[34] B. Tar and A. Fayed, "An overview of the fundamentals of battery chargers," *Midwest Symp. Circuits Syst.*, vol. 10, pp. 16–19, 2016.

[35] F. Eltoumi, *Charging Station for Electric Vehicle Using Hybrid Sources*, Universite Bourgogne Franche-Comte, Dijon, France, 2020.

[36] G. R. C. Mouli, P. Bauer, and M. Zeman, "System design for a solar powered electric vehicle charging station for workplaces," *Applied Energy*, vol. 168, p. 434, 2016.

[37] S. Cheikh-Mohamad, M. Sechilariu, F. Locment, and Y. Krim, "PV-powered electric vehicle charging stations: preliminary requirements and feasibility conditions," *Applied Sciences*, vol. 11, no. 4, p. 1770, 2021.

[38] V. Kumar, V. R. Teja, M. Singh, and S. Mishra, "PV based off-grid charging station for electric vehicle," *IFAC-PapersOnLine*, vol. 52, no. 4, pp. 276–281, 2019.

[39] S. Aliesfahani and M. Shahbazian, "Maximum power point tracking f or solar photovoltaic system using genetic programming toolbox f or identification of physical system," *Journal of Automatic Control*, vol. 3, no. 3, pp. 25–28, 2015.

[40] S. Kim, T. Kim, and J. Choi, "Integrated chip current mode DC-DC buck converter for wireless power receiver," *The International Conference on Electrical Engineering*, vol. 10, no. 10, pp. 1–11, 2016.